Metabolic imprints in the hydrogen isotopes of *Archaeoglobus fulgidus* tetraether lipids

Jeemin H. Rhim[a,*,1], Sebastian Kopf[b], Jamie McFarlin[b,c], Ashley E. Maloney[b], Harpreet Batther[b], Carolynn M. Harris[a], Alice Zhou[a,2], Xiahong Feng[a], Yuki Weber[d,3], Shelley Hoeft-McCann[d,4], Ann Pearson[d], and William D. Leavitt[a,e]

[a] Department of Earth Sciences, Dartmouth College
[b] Department of Geological Sciences, University of Colorado Boulder
[c] Department of Geology & Geophysics, University of Wyoming
[d] Department of Earth & Planetary Sciences, Harvard University
[e] Department of Chemistry, Dartmouth College

* Corresponding author: jrhim@ucsb.edu (J.H. Rhim)

[1] Current address: University of California Santa Barbara, Santa Barbara, CA, USA
[2] Current address: University of Michigan, Ann Arbor, MI, USA
[3] Current address: Chroma Medicine, Boston, MA, USA
[4] Current address: Wellesley College, MA, USA

Keywords: Archaeal lipids, tetraether lipids, GDGTs, biphytanes, hydrogen isotope, biomarkers

Abstract

The stable hydrogen isotope composition of archaeal lipids is emerging as a potential paleoenvironmental proxy, adding to the well-established application of plant leaf wax-derived *n*-alkanes in paleohydrological reconstruction. A handful of studies reported relatively invariant and depleted hydrogen isotope compositions for archaeal lipids despite the range of different organisms and growth conditions explored. However, how modes of metabolism and physiological state (growth phase) affect the hydrogen isotope signatures of archaeal lipids remains poorly understood, limiting our ability to interpret archaeal lipid biomarker records from the environment. Here we conducted water isotope label experiments with a metabolically flexible and well-studied model archaeon *Archaeoglobus fulgidus* and quantified the hydrogen isotope fractionation between lipids and water in response to different carbon substrates and electron donor-acceptor pairs. The $^2H/^1H$ fractionation between lipids and water ($\varepsilon_{L/W}$) was overall negative, ranging from –280 to –226 ‰, and overlapped with the ranges observed for other archaea in previous studies. Isotope flux-balance model results suggest that ≥80 % and ≥50 % of lipid-bound H in *A. fulgidus* cultures directly reflect water isotope compositions (i.e., not via organic substrate or H_2) during autotrophy and heterotrophy, respectively. The model results also suggest the final saturation during isoprenoid lipid biosynthesis catalyzed by a flavoenzyme geranylgeranyl reductase likely contributes to the large $^2H/^1H$ fractionation observed in this study, consistent with previous isotope flux-balance model results for a different archaeon. Finally, we synthesized available data to compare $\varepsilon_{L/W}$ patterns across all three domains of life: Bacteria, Archaea and Eukarya. Emerging patterns between archaeal and eukaryotic lipids are consistent with the notion of highly

fractionating geranylgeranyl reductase, and the patterns between archaeal and bacterial lipids suggest that the general state of energy limitation may also contribute to large, negative values of $\varepsilon_{L/W}$ observed in prokaryotic lipids. Altogether, these findings lend further support for the potential of archaeal lipid $\varepsilon_{L/W}$ as a paleohydrological proxy and provide a broader insight into the $^{2}H/^{1}H$ fractionation mechanisms potentially shared among prokaryotic and eukaryotic lipid biomarkers.

1. Introduction

Hydrogen (H) plays a crucial role in most metabolic processes and is incorporated into biological molecules, often with distinct isotope fractionation patterns. Consequently, the ratio of stable hydrogen isotopes ($^{2}H/^{1}H$) of certain biomolecules can be used to track the H isotope compositions of source water, or the operation of specific biosynthetic pathways (Leavitt et al., 2023). Lipid-bound H in hydrocarbons may resist isotope exchange over geologic time scales for up to 10^4 to 10^8 years (Sessions et al., 2004). Thus, sedimentary records of lipid δ^2H can be applied to reconstruct past ecological or hydrological states (Sachse et al., 2012; Sessions, 2016; McFarlin et al., 2019). The δ^2H of lipids produced by photoautotrophic eukaryotes as well as chemoautotrophic and heterotrophic bacteria have been studied in detail for this reason (e.g., Sessions et al., 1999; Chikaraishi and Naraoka, 2003; Zhang and Sachs, 2007; Zhang et al., 2009; Sachse et al., 2012; Sachs, 2014; Dawson et al., 2015; Osburn et al., 2016; Leavitt et al., 2016; Wijker et al., 2019; McFarlin et al., 2019). In contrast, there are only a handful of studies on the H isotope compositions of archaeal lipids (Kaneko et al., 2011; Dirghangi and Pagani, 2013; Wu et al., 2020; Lengger et al., 2021; Leavitt, Kopf et al., 2023). As a consequence, the factors controlling the lipid/water fractionation ($\varepsilon_{L/W}$), as well as the extent and limits of proxy applications remain poorly understood for archaeal lipids.

The $\varepsilon_{L/W}$ capture a combination of source water δ^2H and the kinetic isotope effect (KIE) of enzymes involved in lipid biosynthesis. For lipids produced by photoautotrophic eukaryotes (e.g., plants and algae), KIE is relatively invariant but can be altered by some environmental factors (e.g., temperature, salinity, irradiance) and some factors intrinsic to an organism (e.g. growth rate in response to different stimuli and underlying genetics) (Sachs, 2014; Van Der Meer et al., 2015; Sachs and Kawka, 2015; Sachs et al., 2016, 2017; Maloney et al., 2016; Bender, 2017; Ladd and Sachs, 2017; Wolfshorndl et al., 2019). In general, these are well studied in eukaryotes, and have been accounted for in hydroclimate proxy studies (Sachse et al., 2012; Sessions, 2016; McFarlin et al., 2019).

Bacterial lipids show a significantly wider range in $\varepsilon_{L/W}$ than eukaryotic lipids. Depending on the central metabolism a given bacteria operates, $\varepsilon_{L/W}$ can range from –400 to –200 ‰ (exclusively negative values) for (an)aerobic chemoautotrophs to –154 to +380 ‰, associated with aerobic heterotrophs (Sessions et al., 2002; Campbell et al., 2009; Zhang et al., 2009; Dawson et al., 2015; Osburn et al., 2016; Leavitt et al., 2016; Wijker et al., 2019). For lipids produced by aerobic heterotrophs, H fluxes through $NADP^+$-reducing and NADPH-balancing reactions provide a quantitative explanation for the full range of $\varepsilon_{L/W}$ values observed (Wijker et al., 2019). Bacterial lipids found in sediments, especially those produced by aerobic heterotrophs, may have more useful applications as proxies for microbial metabolism and ecology rather than past hydroclimate (Zhang et al., 2009; Wijker et al., 2019).

Less is known about what information archaeal $\varepsilon_{L/W}$ record. Studies to-date indicate that archaeal lipids are generally depleted in ^2H, with $\varepsilon_{L/W}$ values similar to those observed in eukaryotic

88 photoautotrophs and bacterial chemoautotrophs (Kaneko et al., 2011; Dirghangi and Pagani, 2013;
89 Wu et al., 2020; Lengger et al., 2021; Leavitt, Kopf et al., 2023). In one recent study, continuous
90 cultures of the obligate autotroph *Nitrosopumilus maritimus* revealed that $\varepsilon_{L/W}$ remains nearly
91 constant across a 3-fold range in growth rate (Leavitt, Kopf et al., 2023). Other studies have
92 reported similarly large, negative values of $\varepsilon_{L/W}$ for archaea grown under heterotrophic conditions
93 (Kaneko et al., 2011; Dirghangi and Pagani, 2013; Wu et al., 2020; Lengger et al., 2021). However,
94 it remains to be determined whether and how carbon metabolism affects $\varepsilon_{L/W}$ within a single
95 organism. Testing this is important, considering that mixotrophy (using both autotrophic and
96 heterotrophic carbon sources) is a widespread mode of metabolism in nature and that many archaea
97 are adapted to fluctuating environments. For bacterial lipids, changes in carbon metabolism
98 resulted in significantly different $\varepsilon_{L/W}$ values within a single organism for some species (e.g.,
99 *Cupriavidus oxalaticus* and *Paracoccus denitrificans*; Zhang et al., 2009; Osburn et al., 2016), but
100 not in other species (sulfate-reducing bacteria; Dawson et al., 2015; Osburn et al., 2016; Leavitt et
101 al., 2016). As such, understanding the role of carbon metabolism in setting archaeal lipid H isotope
102 compositions is important for interpreting archaeal lipid records from the environment.
103 Furthermore, our current understanding of broader patterns of $\varepsilon_{L/W}$ that emerge from comparison
104 across lipids produced by all three domains of life—Archaea, Bacteria, and Eukarya—is limited,
105 despite the similarities observed among certain subgroups of different domains.
106
107 In this study, we conducted pure culture experiments to better understand factors influencing $\varepsilon_{L/W}$
108 in archaeal lipids. To test the effect of metabolism on $\varepsilon_{L/W}$ within a single organism, we cultivate
109 a metabolically flexible archaeon *Archaeoglobus fulgidus* in batch cultures on different carbon
110 substrates and electron donor-acceptor pairs (lactate-thiosulfate, lactate-sulfate, and H_2/CO_2-

111 thiosulfate). We also probe the effect of growth phase by comparing biomass harvested at
112 exponential and stationary growth phases and track the fraction of water incorporated into the final
113 product lipid by using different water isotope compositions of growth media. We then interpret
114 the regression parameters derived from water isotope label experiments with an isotope flux-
115 balance model informed by the enzymatic steps involved in the Wood-Ljungdahl (reductive acetyl-
116 CoA) pathway used by *A. fulgidus* as well as archaeal isoprenoid lipid biosynthesis pathways used
117 by all tetraether-producing archaea. In addition to *A. fulgidus*, we examine two thermoacidophilic
118 archaea (*Acidianus* sp. DS80 and *Metallosphaera sedula* DSM 5348T) for additional $\varepsilon_{L/W}$
119 measurements. We synthesize our new findings in the domain Archaea along with other available
120 archaeal lipid $\varepsilon_{L/W}$ data as well as representative $\varepsilon_{L/W}$ values from domains Bacteria and Eukarya,
121 and highlight factors that underlie patterns in $\varepsilon_{L/W}$ across the three domains of life.

122 ## 2. Materials and Methods

123 ### 2.1. Culture Strains and Growth

124 *Archaeoglobus fulgidus* str. VC-16 (DSM4304) was obtained from Deutsche Sammlung von
125 Mikroorganismen und Zellkulturen (Braunschweig, Germany) and grown in batch cultures on two
126 different carbon substrates and electron acceptors (Table 1). Culture media was prepared following
127 the DSMZ 399 recipe with modifications as follows (per liter): 0.34 g KCl, 4.00 g $MgCl_2 \cdot 6\ H_2O$,
128 3.45 g $MgSO_4 \cdot 7\ H_2O$, 0.25 g NH_4Cl, 0.14 g $CaCl_2 \cdot 2\ H_2O$, 0.11 g $K_2HPO_4 \cdot 3\ H_2O$, 0.20 g KH_2PO_4,
129 18.00 g NaCl, 2.52 g $NaHCO_3$, 2 mL $Fe(NH_4)_2(SO_4)_2 \cdot 7\ H_2O$ (0.1% w/v), and 10 mL trace elements
130 (DSMZ 141). After autoclaving, sterile anoxic solutions were added to the medium to a final
131 concentration of 3.2 mM L-cysteine-HCl and 1% (v/v) vitamin solution (DSMZ 141). When
132 thiosulfate was used as an electron acceptor, 4.00 g/L $MgCl_2 \cdot 6\ H_2O$ and 3.45 g/L $MgSO_4 \cdot 7\ H_2O$

133 were replaced with 4.70 g/L $MgCl_2 \cdot 6\ H_2O$ and 3.48 g/L $Na_2S_2O_3 \cdot 5\ H_2O$. For heterotrophic growth,
134 lactate was used as an electron donor and carbon source, 20 mM of Na-lactate solution was added
135 and incubated with approximately 1 bar of N_2/CO_2 (80:20, v/v) headspace; for autotrophic growth,
136 lactate was omitted and H_2 and CO_2 were used as an electron donor and carbon source,
137 respectively, with 21 psig H_2/CO_2 (80:20, v/v) in the headspace. The headspaces of autotrophic
138 cultures were flushed and re-pressurized with H_2/CO_2 once per day after each OD measurement.
139 The δ^2H of culture media was manipulated by volumetrically diluting 99.9 % purity ^2H_2O.
140
141 All cultures of *A. fulgidus* were incubated at 82 °C. Heterotrophic cultures were incubated
142 statically, and autotrophic cultures were shaken at 200 rpm to increase gas exchange between the
143 H_2/CO_2 headspace and culture media. The optical density at 600 nm (OD_{600}) of samples was used
144 for monitoring growth, and linearity against direct cell counts was confirmed (depth 0.02 mm;
145 Petroff-Hausser Counter 3900) throughout the absorbance range. Biomass samples were harvested
146 twice per experiment, one during mid-exponential phase and the other during early stationary
147 phase. To harvest, 50 mL of culture was centrifuged for 15 minutes at 4 °C and 4500 *g* and resulting
148 wet cell pellets were stored at –80 °C until lipid extraction.
149
150 Batch cultures of *Acidianus* sp. DS80 and *M. sedula* DSM 5348T were grown for additional
151 archaeal lipid $\varepsilon_{L/W}$ measurements (not for water isotope labeling experiments or isotope flux-
152 balance model). *Acidianus* sp. DS80 was grown as previously described in (Rhim, Zhou et al.,
153 2024), and *M. sedula* was grown in Brock basal salts medium with Allen's trace element mixture
154 (Brock et al., 1972). See Supporting Information for additional details for growth conditions for
155 *Acidianus* sp. DS80 and *M. sedula*.

156

157 2.2. Lipid Extraction, Ether Cleavage, and Quantification

158 Frozen cell pellets were lyophilized overnight, and dry cell pellets were extracted using acidic
159 hydrolysis-methanolysis. Briefly, dry cell pellets were physically disrupted in 1.5-mL
160 microcentrifuge tubes by vortexing with methanol (MeOH) and *ca*. 250 µL of 100 µm combusted
161 glass beads for 10 minutes at 3000 rpm using a Disruptor Genie (Scientific 126 Industries, SI-
162 DD38). After excess MeOH wasevaporated, octacosanol (C_{28}) or lignocerol (C_{24}) and C_{46} GTGT
163 were added to all samples as internal extraction standards. Samples were incubated at 65 °C for 90
164 minutes with 3 N methanolic HCl (33 % water content) to hydrolyze tetraether headgroups. Methyl
165 tert-butyl ether (MTBE) was added to the cooled samples at a ratio of 3:2 (acid:MTBE, v/v), and
166 samples were sonicated for 5 minutes (Qsonica Q500, Newtown, CT, USA). After sonication, n-
167 hexane was added at a 1:1 ratio (MTBE:hexane, v/v), vortexed, and centrifuged at 15,000 g for 3
168 minutes. The upper organic phase was collected three times with n-hexane for the two subsequent
169 rounds. The resulting total lipid extracts (TLEs) were dried under N_2 and proceeded to ether
170 cleavage or stored at –20 °C until ether cleavage.

171

172 Ether bonds were cleaved in 57% hydroiodic acid (HI) at 125 °C for 4 hours. Then the organic
173 phase was collected three times using n-hexane. The resulting alkyl iodides were reduced to
174 alkanes (biphytanes, BPs) with H_2 in the presence of $Pt^{(IV)}O_2$ (Kaneko et al., 2011). Hydrogenated
175 samples were passed through combusted pasteur pipettes with glass wool plugs to remove PtO_2
176 powder. Filtered samples were dried under N_2 and stored at –20 °C until analysis. The resulting
177 ether-cleaved BPs were analyzed on a single quadrupole gas chromatography-mass spectrometer
178 (GC-MS; Thermo ISQ LT with TRACE 1310) for compound identification and on a GC-flame

ionization detector (GC-FID; Thermo TRACE 1310) for quantification, both housed in the Organic Geochemistry Laboratory at the University of Colorado Boulder.

2.3. Hydrogen isotope analysis and data processing

The δ^2H of BPs was analyzed on a GC-pyrolysis-isotope ratio MS (GC-P-IRMS) on a GC IsoLink II IRMS System (Thermo Scientific) in the Organic Geochemistry Laboratory at the University of Colorado Boulder. The GC-P-IRMS system consists of a Trace 1310 GC fitted with a programmable temperature vaporization (PTV) injector and either a 30 m ZB5HT column (i.d. = 0.25 mm, 0.25 µm, Phenomenex, Torrance, CA, USA) or a 60 m DB1 column (i.d. = 0.25 mm, 0.25 µm, Agilent, Santa Clara, CA, USA), ConFlo IV interface, and MAT 253 Plus mass spectrometer (Thermo Scientific).

A. fulgidus has been observed to produce both tetraether and diether lipids, with the majority of GDGT with no ring (GDGT-0) and a small fraction with up to two pentacyclic rings (Lai et al., 2008). The tetraether-to-diether ratio for *A. fulgidus* is expected to be ~1:1 at the growth temperature in this study (82 °C; Lai et al., 2008), and we focus on the tetraether fraction for the rest of the discussion. In line with the previous observations, the majority of BPs derived from *A. fulgidus* GDGT did not have rings (BP-0). All δ^2H values reported in this study are for BP-0.

All hydrogen isotope ratios are reported in the standard delta notation (δ^2H) in permil (‰) units, against the Vienna Standard Mean Ocean Water (VSMOW) international standard:

$$\delta\, 2H = \left[\frac{(2H/1H)_{sample}}{(2H/1H)_{VSMOW}} - 1\right] \times 1000 \qquad \text{Eq. (1)}$$

The lipid-water hydrogen isotope fractionation factor is reported in alpha notation ($^2\alpha_{L/W}$), and fractionation is reported in epsilon notation ($^2\varepsilon_{L/W}$) in ‰:

$$2\alpha_{L/W} = \frac{(2H/1H)_{lipid}}{(2H/1H)_{water}} \qquad \text{Eq. (2)}$$

$$2\varepsilon_{L/W} = \left[2\alpha_{L/W} - 1\right] \times 1000 \qquad \text{Eq. (3)}$$

Values of δ^2H were first determined relative to H_2 reference gas (δ^2H_{raw}), and then calibrated externally using a standard *n*-alkane mixture (A6, containing C_{15} through C_{30} n-alkanes spanning –9 to –263 ‰ vs. VSMOW; A. Schimmelmann, Indiana University). The A6 standard was combined with a C_{36} n-alkane (nC_{36}, –259.2 ‰ vs. VSMOW; A. Schimmelmann, Indiana University) and measured at regular intervals at different concentrations. The BP δ^2H calibration was done in R, using the packages *isoreader* (Kopf et al., 2021) and *isoprocessor* available at github.com/isoverse. Details of the data reduction and calibration methods are described in (Leavitt, Kopf et al., 2023). The RMSE of the calibration peaks was 4.2 ‰ (n=613) across a peak size range from 6.2 to 59.9 Vs. The RMSE of the C_{36} *n*-alkane internal standard was 7.5 ‰ (n=90) across a peak size range from 6.4 to 50.9 Vs. Calibrated δ^2H values for the biphytanes were corrected for the H added during hydrogenation of alkyl iodides (see Leavitt, Kopf et al., 2023). The hydrogenation correction ranged from 9.8 to 13.7 ‰ and increased analytical uncertainty by up to 1.8 ‰.

The δ^2H of the H_2 gas in the H_2/CO_2 headspace of autotrophic cultures was analyzed on a Thermo Gasbench II in the Stable Isotope Laboratory at Northwestern University. The δ^2H of non-exchangeable H in lactate used for heterotrophic cultures was assumed to be –60 ‰, which is the value previously determined for glucose (Zhang et al., 2009).

The δ^2H of natural abundance and deuterium-enriched medium water was measured at the Stable Isotope Laboratory at Dartmouth College as previously described (Kopec et al., 2019). Briefly, water was reduced with chromium at 850 °C using the H-Device, and the δ^2H of the resulting gas was measured by an IRMS (Thermo Delta Plus XL). The measured δ^2H values were converted to the water δ^2H equivalent by calibrating with water standards with known isotopic compositions analyzed in the same way. For samples expected to be outside the range of the standards (e.g., the deuterium-enriched medium), samples were diluted with water standards. The 1σ uncertainty for δ^2H measurements is <0.5 ‰.

2.4. Model implementation

An isotope flux-balance model was adapted from the conceptual framework described in Leavitt, Kopf et al. (2023). Our model considers the Wood-Ljungdahl (reductive acetyl-CoA) pathway used by A. fulgidus for determining the sources and fluxes of H during acetyl-CoA (Ac-CoA) synthesis. It also considers the general archaeal lipid biosynthesis pathway for the accounting of total H budget in archaeal lipids. Analytical solutions for the model were calculated in R. Details of the model design and outcomes are described in section 4.

3. Results

3.1. Cultures and growth rates

Archaeoglobus fulgidus is a metabolically flexible strain from the phylum Euryarchaeota. We cultivated *A. fulgidus* in batch (closed-system) cultures on three different combinations of electron donors and acceptors (Table 1; Fig. 1A–C). In two treatments, *A. fulgidus* was grown as a heterotroph, using lactate as the carbon source and electron donor and sulfate or thiosulfate as the

terminal electron acceptor. In the third treatment, *A. fulgidus* was grown as an autotroph, using CO_2 as the carbon source, H_2 as the electron donor, and thiosulfate as the terminal electron acceptor. Cultures were acclimated to each treatment by growing on respective substrate combinations for two or more passages before inoculation. Overall, heterotrophic conditions resulted in faster growth (T-L, t_d = 6.2 ± 0.6 h; S-L, t_d = 10.3 ± 1.7 h) compared to autotrophic growth (T-H_2/CO_2, t_d = 19.3 ± 3.9 h) (Table 2; Fig. 1A–C).

Table 1. Summary of culture experiments.

Experimental Condition	electron donor	electron acceptor	carbon source
Thiosulfate-Lactate (T-L)	Lactate (20 mM)	Thiosulfate (14 mM)	Lactate (20 mM)
Sulfate-Lactate (S-L)	Lactate (20 mM)	Sulfate (14 mM)	Lactate (20 mM)
Thiosulfate-H_2/CO_2 (T-H_2/CO_2)	H_2 (g)* (80% v/v)	Thiosulfate (14 mM)	CO_2 (g)* (20% v/v)

* The headspace of autotrophic cultures was filled with 21 psig H_2/CO_2 (80:20, v/v) and re-pressurized with H_2/CO_2 once per day after each OD measurement.

3.2. Carbon metabolism and growth phase affect lipid δ^2H and regression parameters

Different modes of carbon metabolism in *A. fulgidus* not only resulted in different growth rates but also affected lipid δ^2H and regression parameters. The lipid isotopic composition reflects the sum of distinct isotope fractionations between lipids and each external H source, resulting in the isotopic mass balance (Zhang et al., 2009):

$$R_{BP} = f_W \cdot 2\alpha_{L/W} \cdot R_W + f_S \cdot 2\alpha_{L/S} \cdot R_S \qquad \text{Eq. (4)}$$

where R_{BP}, R_W, and R_S represent the $^2H/^1H$ ratios of BPs from GDGT-0 (BP-0), media water, and substrate (lactate for the heterotrophic conditions; H_2 for the autotrophic condition), respectively. f_W and f_S are the fractions of lipid-bound H originating from water and substrate, respectively. $^2\alpha$

represents the net isotope fractionation factor between lipid and water ($^2\alpha_{L/W}$) and between lipid and substrate ($^2\alpha_{L/S}$), respectively. In parallel cultures where only one parameter (R_W) is varied experimentally, measurements of R_L, R_W, and R_S provide the basis for regression of R_L on R_W. The isotope analysis results and regression parameters are summarized in Table 2.

The δ^2H_L values were strongly correlated with δ^2H_W values in all experiments (Table 2; $R^2 \geq 0.993$ and $p \leq 0.05$ in every regression). The regression slopes varied as a function of carbon metabolism and growth phase. Overall, the two heterotrophic conditions (T-L and S-L) and exponential growth phase resulted in lower slopes compared to the autotrophic condition (T-H_2/CO_2) and stationary growth phase. Slopes for the two heterotrophic conditions were similar (0.481 ± 0.017 for T-L, 0.477 ± 0.028 for S-L during exponential phase; 0.548 ± 0.015 for T-L, 0.519 ± 0.016 for S-L during stationary phase; Table 2). The autotrophic condition resulted in higher slopes (0.552 ± 0.019, exponential phase; 0.628 ± 0.025, stationary phase; Table 2). Notably, the higher slope observed during the stationary phase of the autotrophic culture was the closest to the slope estimated assuming $f_W = 1$ (0.707) (Table 2; Fig. 1D).

Table 2. Growth and isotope data for tetraether-derived biphytanes produced by *Archaeoglobus fulgidus* grown on different carbon substrates and electron donor-acceptor pairs.

Substrate[a]	t_d (h)[b]	Growth Phase[c]	Avg. OD[d]	δ^2H_W[e] (‰)	s.d. (‰)	δ^2H_L[f] (‰)	s.d. (‰)	$^2\varepsilon_{L/W}$ (‰)	s.d. (‰)	n[g]	Slope[h] ($^2\alpha_{L/W} \cdot f_W$)	s.e.	R^2	*p*
T-L	6.2 ± 0.6	Exp	0.147	362.4	0.2	–70.7	6.6	–317.9	29.4	3	0.481	0.017	0.996	1×10^{-7}
			0.135	176.0	0.2	–164.6	7.0	–289.6	12.4	3				
			0.141	–64.0	0.2	–275.8	7.1	–226.2	5.9	2				
		Sta	0.346	361.3	0.2	–52.7	6.7	–304.1	38.5	2	0.548	0.015	0.999	3×10^{-6}
			0.344	175.5	0.2	–152.4	7.5	–279.0	13.7	2				
			0.351	–63.7	0.2	–285.3	8.7	–236.7	7.2	2				
S-L	10.3 ± 1.7	Exp	0.096	361.8	0.2	–87.5	9.7	–329.9	36.4	1	0.477	0.028	0.993	7×10^{-5}
			0.100	174.7	0.2	–163.5	4.8	–287.9	8.5	3				
			0.082	–61.7	0.2	–289.7	5.9	–243.0	5.0	2				
		Sta	0.307	361.4	0.2	–66.9	5.7	–314.6	26.9	2	0.519	0.016	0.998	4×10^{-7}
			0.295	175.4	0.2	–168.1	4.9	–292.3	8.5	2				
			0.282	–61.5	0.2	–287.1	10.2	–240.3	8.6	2				
T-H_2/CO_2	19.3 ± 3.9	Exp	0.052	348.3	0.2	–72.8	5.0	–312.3	21.5	2	0.552	0.019	0.998	8×10^{-5}
			0.046	164.8	0.2	–176.8	7.0	–294.0	11.5	1				
			0.054	–66.5	0.2	–302.1	4.7	–252.4	4.0	1				
		Sta	0.137	348.5	0.2	–71.7	8.7	–311.7	37.8	3	0.628	0.025	0.997	1×10^{-5}
			0.132	166.0	0.2	–173.8	10.0	–291.4	16.8	1				
			0.134	–64.5	0.2	–326.4	10.2	–279.9	8.8	2				
T-H_2/CO_2 (calculated)		-	-	-	-	-	-	-	-	-	*0.707 (f_W = 1)*	-	-	-

[a] Thiosulfate-lactate (T-L); sulfate-lactate (S-L); thiosulfate-H_2/CO_2 (T-H_2/CO_2)
[b] Doubling time calculated for logarithmic growth
[c] Biomass harvested during mid-exponential growth phase (Exp); biomass harvested during early stationary phase, including biomass from both exponential and stationary phase (Sta)
[d] Optical density (OD)
[e] δ^2H of culture medium at the time of biomass sampling. Average of biological and technical replicates ± 1 s.d.
[f] Weighted mean δ^2H of biphytane from GDGT-0
[g] Number of biological replicates used to calculate the average values of δ^2H_{Water}, δ^2H_{Lipid}, and $^2\varepsilon_{L/W}$
[h] Slope for the regression of δ^2H_{Lipid} against δ^2H_{Water} (*see* Figure 1D-F)

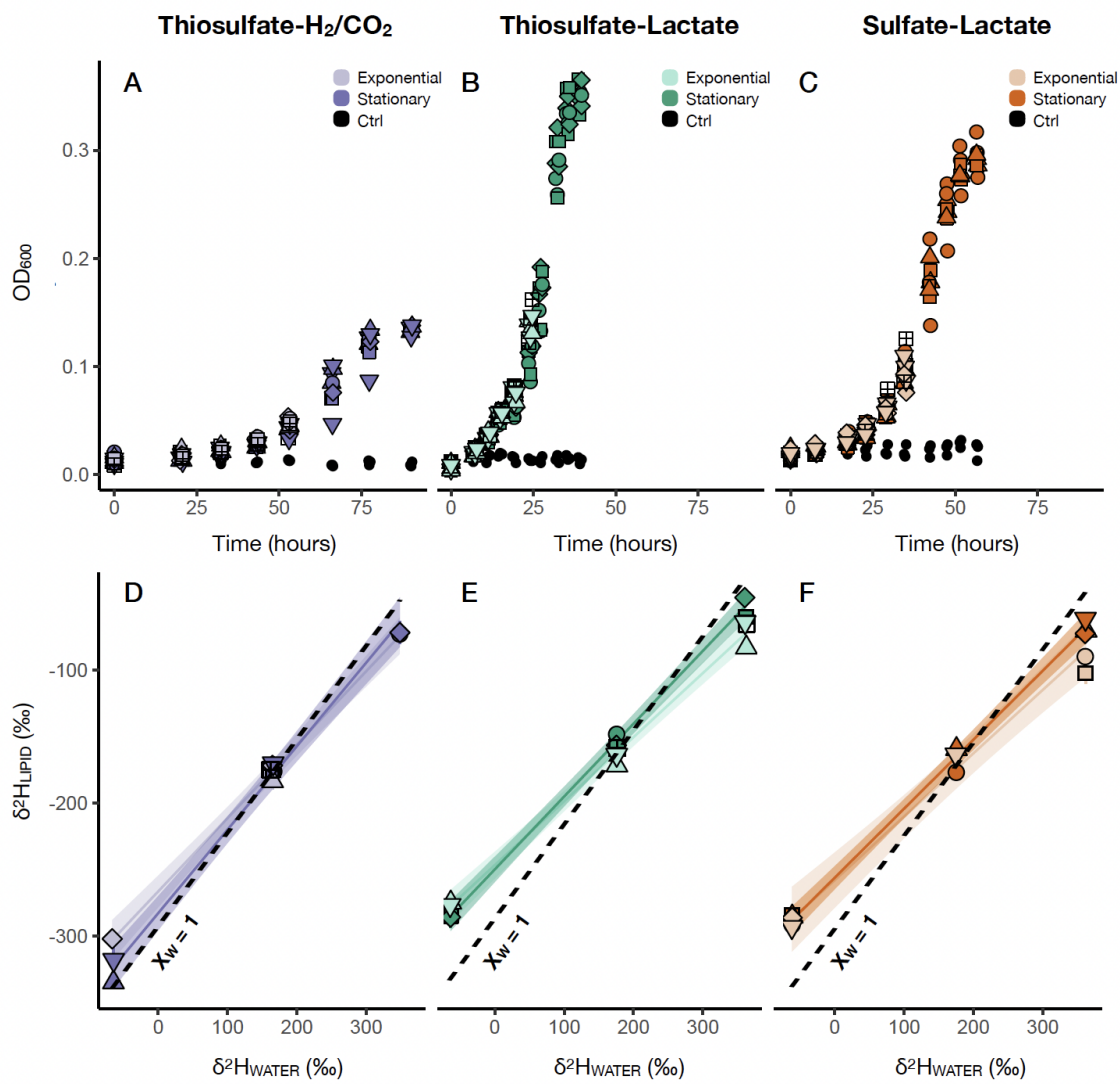

Figure 1. Growth curves and regression of lipid δ^2H versus water δ^2H for *Archaeoglobus fulgidus*. Growth curves of *A. fulgidus* grown autotrophically on (A) thiosulfate and H_2/CO_2 or heterotrophically on (B) thiosulfate and lactate or (C) sulfate and lactate. Regression of biphytane hydrogen isotopic composition (δ^2H_L) on water isotopic composition (δ^2H_W) grown on (D) thiosulfate and H_2/CO_2, (E) thiosulfate and lactate, and (F) sulfate and lactate.

4. *A. fulgidus* H-isotope flux-balance model

To further interpret these findings, we modified the isotope flux-balance model recently developed for an ammonia-oxidizing archaeon *N. maritimus* SCM1 (Leavitt, Kopf et al., 2023) to reflect the biochemistry underlying the different modes of carbon metabolism in *Archaeoglobus fulgidus* VC-16. The overall conceptual framework consists of two parts for the stoichiometric accounting of:

305 1) methyl-H in Ac-CoA and 2) the 80 H atoms in the C_{40} alkyl chain of BPs inherited from Ac-
306 CoA. The former requires metabolism-specific information considering the mode(s) of carbon
307 fixation and experimental conditions such as substrate availability, while the latter is informed by
308 more universal information about archaeal isoprenoid biosynthesis. Below, we describe the details
309 of the two parts of our model.
310

311 ## 4.1. Sources of lipid-H via the modified Wood-Ljungdahl pathway

312 ### *4.1.1. Heterotrophy*

313 *A. fulgidus* can grow autotrophically or heterotrophically via the modified reductive Ac-CoA or
314 Wood-Ljungdahl pathway (Möller-Zinkhan et al., 1989; Möller-Zinkhan and Thauer, 1990;
315 Hocking et al., 2014). During chemoorganoheterotrophic growth on lactate, the type species *A.*
316 *fulgidus* VC16 couples the complete oxidation of organic substrates to CO_2 with the reduction of
317 sulfate or thiosulfate to sulfide. In this study, the organic substrate was lactate. *A. fulgidus* oxidizes
318 lactate via pyruvate and Ac-CoA using enzymes and cofactors involved in the C_1-pathway, similar
319 to those found in methanogens, in reverse direction (Fig. 2A; Möller-Zinkhan et al., 1989; Möller-
320 Zinkhan and Thauer, 1990). A D-lactate dehydrogenase in *A. fulgidus* catalyzes the first step of
321 lactate oxidation to pyruvate coupled with the reduction of menaquinone (MQ), resulting in
322 menaquinol (MQH_2) (Step 1, Fig. 2A; Kunow et al., 1993; Reed and Hartzell, 1999). The next step
323 of pyruvate oxidation to Ac-CoA is catalyzed by pyruvate:ferredoxin oxidoreductase (Step 2, Fig.
324 2A; Kunow et al., 1993). The three H atoms in the methyl group of lactate most likely remain
325 intact and are inherited to Ac-CoA. Some of these Ac-CoA products are used for biomass synthesis
326 (Step 3.2, Fig. 2A), including isoprenoid lipid biosynthesis, while some of them are degraded
327 further for the complete oxidation of lactate. For the latter, carbon monoxide dehydrogenase

328 catalyzes both the reversible carbon-carbon cleavage of Ac-CoA and the oxidation of carbonyl
329 group to CO_2 coupled with ferredoxin (Fd) reduction (Step 3.1, Fig. 2A; Möller-Zinkhan and
330 Thauer, 1990).
331
332 The coenzymes involved in the downstream oxidative branch of Ac-CoA degradation could
333 transfer hydrides (e.g., $F_{420}H_2$ in Steps 4 and 5, Fig. 2A). These fluxes of H are important to track
334 because the hydrides from Ac-CoA (ultimately from lactate) can be recycled for NADP reduction,
335 the product of which (NADPH) can donate hydrides to isoprenoid precursors during lipid
336 biosynthesis. We assign F_{420} and Fd as the electron acceptors for Steps 4–5 and Step 8, respectively
337 (Fig. 2A), given that the genes relating to all steps of the reductive Ac-CoA pathway are expressed
338 in *A. fulgidus* (Hocking et al., 2014) and considering the known mechanisms of how the enzymes
339 of interest operate in methanogens. In CO_2-reducing methanogens, both
340 methylenetetrahydromethanopterin reductase (Mer) and methylenetetrahydromethanopterin
341 dehyrogenase (Mtd) oxidize $F_{420}H_2$ (Steps 4 and 5, respectively, in reverse; Fig. 2A), and
342 formylmethanofuran dehydrogenase (Fwd) requires Fd_{red} (Step 8, in reverse; Fig. 2A) (Thauer,
343 2012).
344
345 *4.1.2. Autotrophy*
346 During chemolithoautotrophic growth *A. fulgidus* VC16 couples H_2 or formate oxidation with
347 thiosulfate or sulfite reduction (Achenbach-Richter et al., 1987; Steinsbu et al., 2010). We fed *A.*
348 *fulgidus* H_2 and thiosulfate as the electron donor and acceptor for the autotrophic condition (T-
349 H_2/CO_2). *A. fulgidus* reduces CO_2 to synthesize Ac-CoA via the C_1-pathway (Fig. 2B), in principle
350 a reversal of the Ac-CoA degradation during heterotrophy (Fig. 2A). The same enzymes involved

in H additions used by CO_2-reducing methanogens catalyze the successive addition of H during autotrophic carbon fixation in *A. fulgidus*: Fwd (Step 1), Mtd (Step 4), and Mer (Step 5) (Fig. 2B). During chemolithoautotrophy, the H atoms in methyl precursors in theory derive from intracellular water. However, one of the isoenzymes for methylenetetrahydromethanopterin (CH_2-H_4MPT) dehydrogenase is H_2-dependent (Hmd) and uses H_2 directly, as opposed to $F_{420}H_2$ used by the other isoenzyme Mtd, to reduce methyl-H_4MPT (Hendrickson and Leigh, 2008). Given the similarities between methanogens and *A. fulgidus*, we consider the possible flux of H from H_2 to Ac-CoA (Step 4–6, Fig. 2B) in one of the end-member scenarios (see 4.2; Table 3).

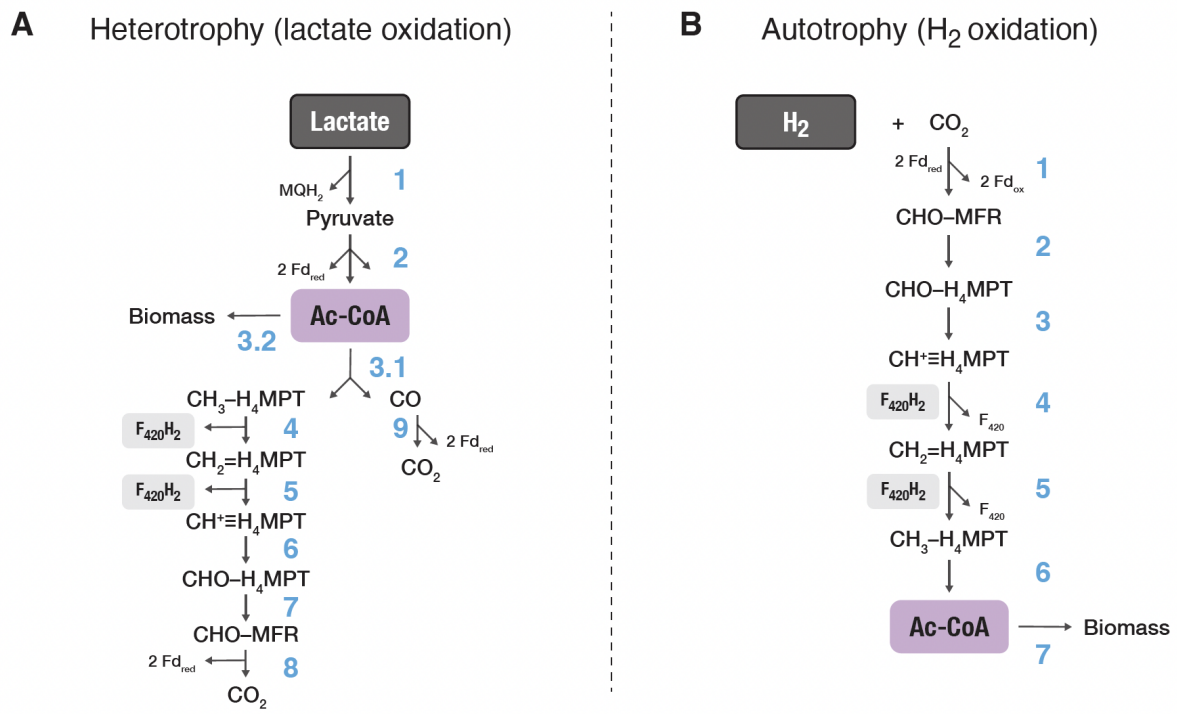

Figure 2. Carbon metabolism by *Archaeoglobus fulgidus* via the modified reductive acetyl-CoA or Wood-Ljungdahl pathway. (A) Chemoorganoheterotrophic growth on lactate: lactate is oxidized via pyruvate and acetyl-CoA, which either serves as the building blocks for biosynthesis or is further degraded for the complete oxidation of lactate. (B) Chemolithoautotrophic growth on H_2/CO_2: CO_2 is reduced to produce acetyl-CoA via the C_1-pathway, with enzymes and cofactors similar to those involved in methanogenesis. Abbreviations: MQH_2, menaquinol or reduced menaquinone; Fd_{red}, reduced ferredoxin; Ac-CoA, acetyl-CoA; CH_3-H_4MPT, methyl-tetrahydromethanopterin (H_4MPT); CH_2=H_4MPT, methylene-H_4MPT; CH^+≡H_4MPT, methenyl-H_4MPT; CHO-H_4MPT, formyl-H_4MPT; CHO-MFR, formylmethanofuran; $F_{420}H_2$, reduced coenzyme F_{420}.

4.2. Model schematics and stoichiometric accounting

Fractions of Ac-CoA produced via the modified Wood-Ljungdahl pathway described above are used for the synthesis of archaeal isoprenoids. Leavitt, Kopf et al. (2023) provide a detailed overview of the sources of H and mechanisms of the biochemical steps involved in archaeal tetraether biosynthesis (Appendix B). In short, the mevalonate pathway synthesizes isopentenyl pyrophosphate (IPP), which are C_5 isoprene units, from three units of Ac-CoA. Then, three units of IPP and its isomer condense to yield the C_{20} precursor, geranylgeranyl diphosphate (GGPP). The geranylgeranyl chains are transferred around to yield di-O-geranylgenranylglyceryl phosphate (DGGGP) with the glycerol-1-phosphate (G1P) backbone. The tetraether synthase (Tes) enzyme catalyzes the condensation of two DGGGP units to yield the membrane-spanning tetraether. Finally, the geranylgeranyl reductase (GGR) enzyme catalyzes the saturation of tetraether to yield GDGT. We combine the stoichiometric accounting of the methyl-H in Ac-CoA for *A. fulgidus* (see 4.1) and of the 80 H atoms in the C_{40} alkyl chain of BPs inherited from Ac-CoA during tetraether biosynthesis described above (Leavitt, Kopf et al., 2023) to build an overall schematic of the specific model scenarios explored in this study (Fig. 3).

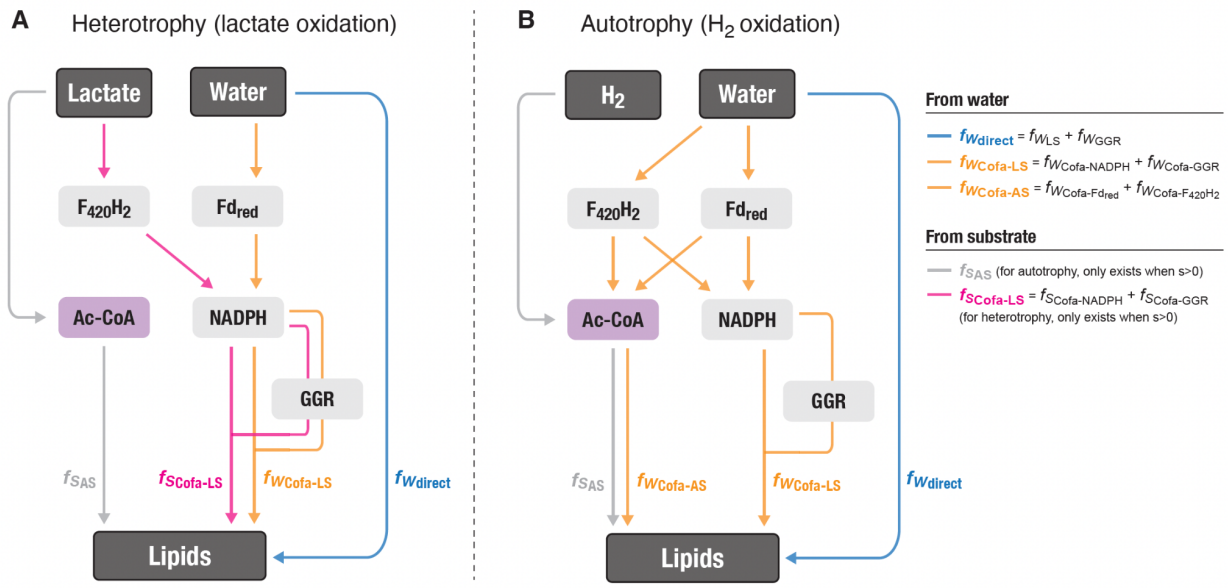

Figure 3. Schematic diagram of the isotope flux-balance model for *Archaeoglobus fulgidus*. (A) Heterotrophic scenario for lactate oxidation; (B) autotrophic scenario for H_2 oxidation. Color codes for the different H fluxes (*f*) are shown in the legend. The subscript W stands for water as the ultimate H source; the subscript S stands for substrate as the ultimate H source, where the substrates are lactate and H_2 for heterotrophy and autotrophy, respectively. See 4.2.1 and Appendix A (Eq. A5–A8) for detailed descriptions of individual fluxes. Abbreviations: LS, lipid synthesis; AS, acetyl-CoA synthesis; Cofa, cofactor; $F_{420}H_2$, reduced coenzyme F_{420}; Fd_{red}, reduced ferredoxin; Ac-CoA, acetyl-CoA; GGR, geranylgeranyl reductase.

4.2.1. Empirically informed isotopic mass balance

With the fractions defined in the overall hydrogen budget (see Appendix A), the isotopic mass balance in Eq. (4) can be further refined. Replacing the f_W and f_S terms in Eq. (4) with the sums of all fractions in Eq. (A5) (Appendix A), isotopic mass balance for the heterotrophic case becomes:

$$R_{BP,het} = \left(f_{W,direct} \cdot \alpha_{W,direct} + f_{W,cofa-LS} \cdot \alpha_{W,cofa-LS}\right) \cdot R_W + \left(f_{S,cofa-LS} \cdot \alpha_{S,cofa-LS} + f_{S,AS} \cdot \alpha_{S,AS}\right) \cdot R_S \qquad \text{Eq. (5)}$$

Similarly, isotopic mass balance for the autotrophic case becomes:

$$R_{BP,auto} = \left(f_{W,direct} \cdot \alpha_{W,direct} + f_{W,cofa-AS} \cdot \alpha_{W,cofa-AS} + f_{W,cofa-LS} \cdot \alpha_{W,cofa-LS}\right) \cdot R_W + f_{S,AS} \cdot \alpha_{S,AS} \cdot R_S$$

Eq. (6)

Now we can use the regression parameters estimated from the δ^2H_{H2O} label experiments (Fig. 1; Table 2) to calculate analytical solutions for reasonable ranges of individual terms in Eq. (5–6). In Eq. (5–6), the coefficient for R_W in the first term represents the slope, *m*, and the entire second term represents the intercept, *c*. For heterotrophy:

$$m_{het} = f_{W,net} \cdot \alpha_{W,net} = f_{W,direct} \cdot \alpha_{W,direct} + f_{W,cofa-LS} \cdot \alpha_{W,cofa-LS}$$

$$\varepsilon_{W,net} = \frac{m_{het}}{f_{W,net}} - 1 = \frac{f_{W,direct} \cdot \alpha_{W,direct} + f_{W,cofa-LS} \cdot \alpha_{W,cofa-LS}}{f_{W,net}} - 1$$

Eq. (7)

$$c_{het} = f_{S,net} \cdot \alpha_{S,net} \cdot R_S = f_{S,cofa-LS} \cdot \alpha_{S,cofa-LS} + f_{S,AS} \cdot \alpha_{S,AS}$$

$$\varepsilon_{S,net} = \frac{c_{het}}{f_{S,net} \cdot R_S} - 1 = \frac{f_{S,cofa-LS} \cdot \alpha_{S,cofa-LS} + f_{S,AS} \cdot \alpha_{S,AS}}{f_{S,net}} - 1$$

Eq. (8)

where $\varepsilon_{W,net}$ and $\varepsilon_{S,net}$ refer to the net isotope fractionation between water and lipid (combining isotope effects associated with $f_{W,direct}$ and $f_{W,cofa-LS}$) and between substrate and lipid (combining isotope effects associated with $f_{S,cofa-LS}$ and $f_{S,AS}$), respectively.

4.3. Model results

Table 3, Fig. 4 and Fig. 5 show the summary of model results. We first estimated $f_{W,net}$, which we define as the total flux that directly or indirectly (e.g., via cofactors) reflects water isotope composition (i.e., not affected by substrate isotopic composition) ($f_{W,net} = f_{W,direct} + f_{W,cofa}$), for a range of x_{ex} from 0 % to 100 %. Overall, the autotrophic case had a higher range of $f_{W,net}$ compared to the two heterotrophic cases (Table 3; Fig. 4A–C). Even for the minimal water exchange and maximal substrate contribution scenario (x_{ex} = 0 %, s = 100 %), when the contribution from

427 substrate is expected to be the highest, $f_{W,net}$ was 80 % (Table 3; dashed line, Fig. 4A). For the two
428 heterotrophic cases, the $f_{W,net}$ values were 31 and 70 % for the highest (x_{ex} = 0 %, s = 100 %) and
429 lowest (x_{ex} = 100 %, s = 0 %) substrate contribution scenarios, respectively (Table 3; Fig. 4B–C).
430
431 For the net isotope fractionation between lipid and water ($\varepsilon_{W,net}$), the two heterotrophic cases
432 showed similar ranges and patterns where the $\varepsilon_{W,net}$ values decrease with increasing x_{ex} (Fig. 4E–
433 F). The $\varepsilon_{W,net}$ range was relatively more positive during stationary growth phase (–218 to 776 ‰
434 for the T-L condition; –259 to 682 ‰ for the S-L condition) compared to exponential growth phase
435 (–312 to 561 ‰ for the T-L condition; –319 to 546 ‰ for the S-L condition) (Table 3: Fig. 4E–F).
436 For the autotrophic case, the growth phase-dependent trend was also observed (more positive $\varepsilon_{W,net}$
437 during stationary phase; Table 3; Fig. 4D). Unlike in the heterotrophic cases, all $\varepsilon_{W,net}$ values for
438 the autotrophic case were negative and fell within a relatively narrow range for the entire range of
439 x_{ex} (–448 to –312 ‰ for exponential phase; –372 to –228 ‰ for stationary phase; Table 3). For the
440 autotrophic case, a theoretical end-member $\varepsilon_{W,net}$ with no substrate contribution can be estimated
441 by calculating the regression slope through the origin (i.e., no intercept, which represents the
442 substrate contribution term, $f_S \cdot {}^2\alpha_{L/W} \cdot R_S$; Eq. (4)): –293 ‰ for the autotrophic case (black dotted
443 line; Fig. 4D). This value falls within the range of $\varepsilon_{W,net}$ for stationary, rather than exponential,
444 growth phase (Fig. 4D). For the net isotope fractionation between lipid and substrate ($\varepsilon_{S,net}$), the
445 two heterotrophic cases showed similar ranges and patterns where $\varepsilon_{S,net}$ values increase with
446 increasing x_{ex} (Fig. 4H–I). The growth phase-dependent trend for $\varepsilon_{S,net}$ contrasted that of $\varepsilon_{W,net}$,
447 where the $\varepsilon_{S,net}$ range was relatively more negative during stationary growth phase (–688 to –282
448 ‰ for the T-L condition; –654 to –201 ‰ for the S-L condition) compared to exponential growth
449 phase (–582 to –36 ‰ for the T-L condition; –592 to –59 ‰ for the S-L condition) (Table 3; Fig.

450 4H–I). A similar trend was observed for the autotrophic case (more negative $\varepsilon_{S,net}$ during stationary
451 phase; Table 3; Fig. 4G).
452
453 The net isotope fractionation factors ($\varepsilon_{W,net}$ and $\varepsilon_{S,net}$) can be further broken down into individual
454 fluxes associated with H isotopes with different routes of incorporation. The net isotope
455 fractionation factor between lipid and water ($\varepsilon_{W,net}$) can be divided into: 1) $\varepsilon_{W,direct}$ associated with
456 H atoms that are transferred through the $f_{W,direct}$ flux (Fig. 3) via H exchange between isoprenoid
457 precursors and intracellular water or addition via GGR, and 2) $\varepsilon_{W,cofa}$ associated with the $f_{W,cofa}$
458 flux ($f_{W,cofa\text{-}LS}$ for heterotrophy; $f_{W,cofa\text{-}LS}$ and $f_{W,cofa\text{-}AS}$ for autotrophy; Fig. 3) via cofactors (Fd_{red}
459 and $F_{420}H_2$ for autotrophy; Fd_{red} for heterotrophy) (Fig. 5A–C). The net isotope fractionation factor
460 between lipid and substrate ($\varepsilon_{S,net}$) can be divided into: 1) $\varepsilon_{S,AS}$ associated with H atoms that are
461 transferred through the $f_{S,AS}$ flux (Fig. 3) via Ac-CoA synthesis, and 2) $\varepsilon_{S,cofa}$ associated with the
462 $f_{S,cofa}$ flux ($f_{S,cofa\text{-}NADPH}$ and $f_{S,cofa\text{-}GGR}$ for heterotrophy; Fig. 3) via cofactors ($F_{420}H_2$) (Fig. 5D–E).
463 Interpretation of these results are discussed further in 5.2.1.
464

465 **Table 3.** Isotope flux-balance model results for *Archaeoglobus fulgidus*.

Growth phase	Scenario		$f_{W,net}$ (%)[c]			$\varepsilon_{W,net}$ (‰)[d]			$\varepsilon_{S,net}$ (‰)[e]		
	x_{ex} (%)[a]	s (%)[b]	T-L	S-L	T-H	T-L	S-L	T-H	T-L	S-L	T-H
Exp.	0	0	41	41	100	179	167	–448	–511	–523	n/a
	0	100	31	31	80	561	546	–312	–582	–592	–564
	100	0	70	70	100	–312	–319	–448	–36	–59	n/a
	100	100	60	60	90	–198	–206	–387	–277	–294	–139
Sta.	0	0	41	41	100	341	270	–372	–636	–595	n/a
	0	100	31	31	80	776	682	–218	–688	–654	–785
	100	0	70	70	100	–218	–259	–372	–282	–201	n/a
	100	100	60	60	90	–87	–136	–302	–461	–401	–577

466
467 [a] the degree of water exchange during lipid synthesis, which depends on the extent of re-equilibration during
468 isomerization steps (Steps 2 and 6; Appendix B).
469 [b] the degree of H contribution to lipids from substrate (lactate for heterotrophy; H_2 for autotrophy)
470 [c] the net total contribution of H from water to lipids ($f_{W,net} = f_{W,direct} + f_{W,cofa}$)
471 [d] the net isotope fractionation between water and lipid (combining isotope effects associated with $f_{W,direct}$ and $f_{W,cofa\text{-}LS}$)
472 [e] the net isotope fractionation between substrate and lipid (combining isotope effects associated with $f_{S,cofa\text{-}LS}$ and $f_{S,AS}$)

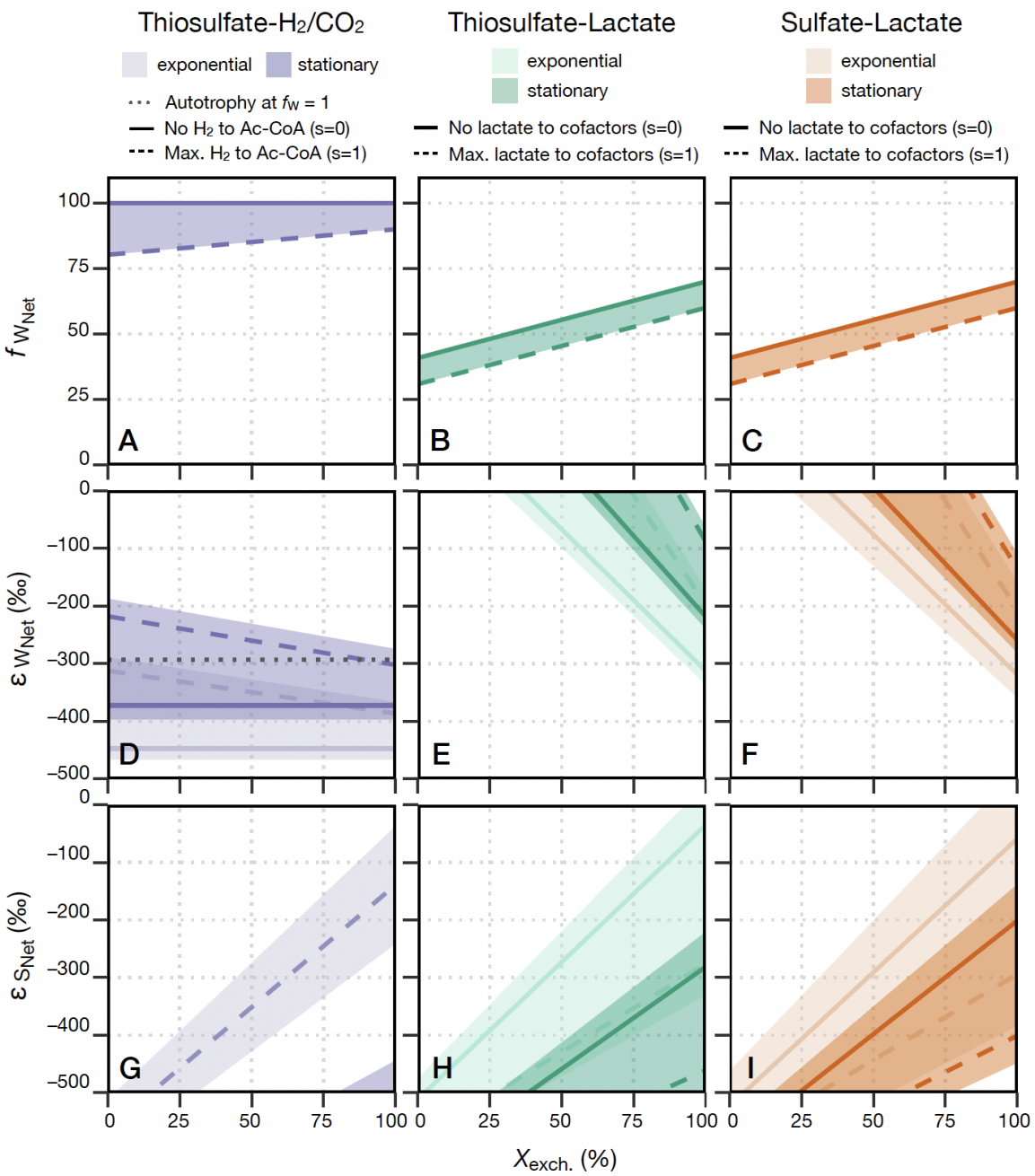

Figure 4. Isotope flux-balance model results for *Archaeoglobus fulgidus*. (A–C) The total flux that directly or indirectly (e.g., via cofactors) reflects water isotope composition (i.e., not affected by substrate isotopic composition) ($f_{W,net}$); (D–F) Net isotope fractionation between lipid and water ($\varepsilon_{W,net}$); (G–I) Net isotope fractionation between lipid and substrate ($\varepsilon_{S,net}$). Each column represents the metabolic mode and growth substrates: autotrophy on thiosulfate and H_2/CO_2 (A, D and G); heterotrophy on thiosulfate and lactate (B, E and H); and heterotrophy on sulfate and lactate (C, F and I). Lighter shaded areas refer to exponential growth phase; darker shades refer to stationary growth phase. Solid lines refer to the s = 0 % (minimal substrate contribution) scenarios; dashed lines refer to the s = 100 % (maximal substrate contribution) scenarios. See 4.2.1 and Table 3 for details of the conditions for each scenario.

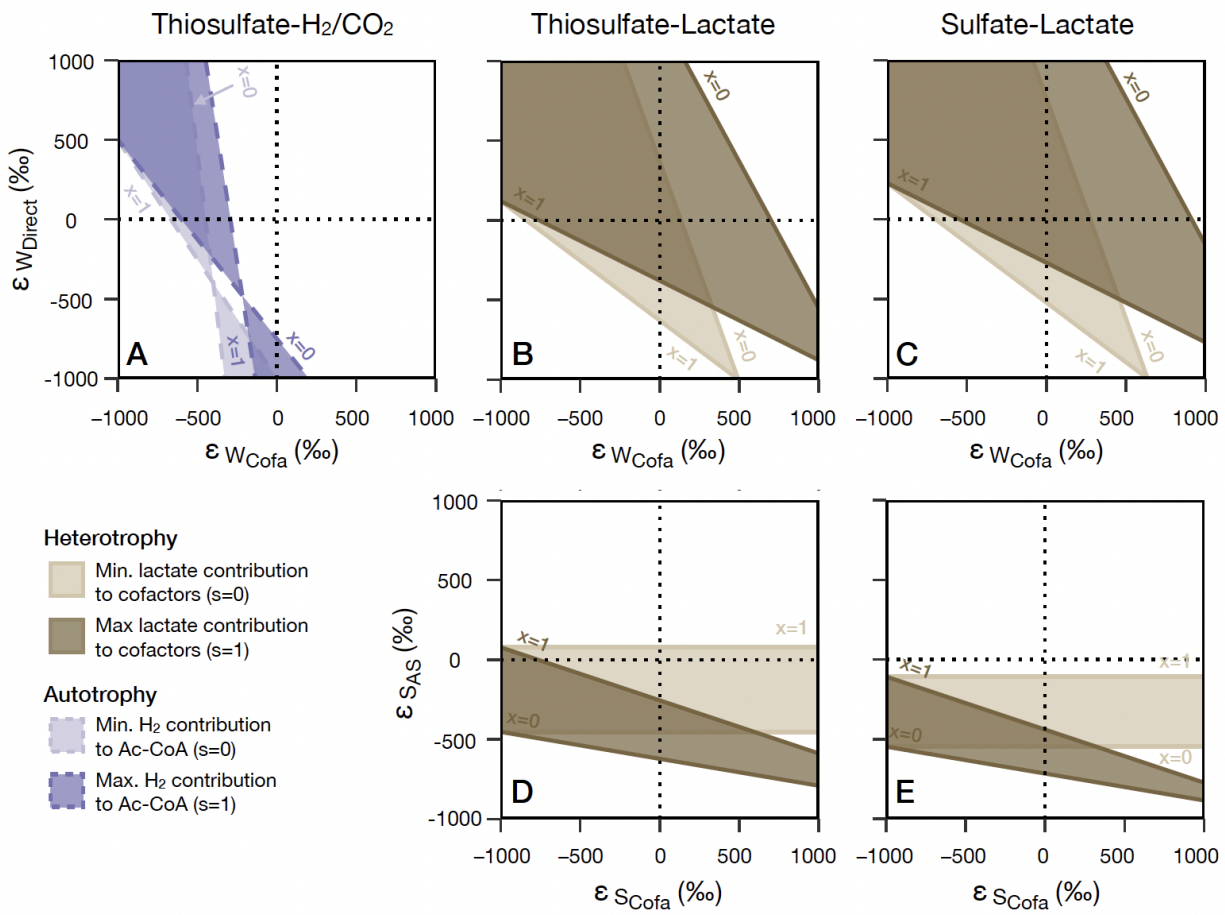
Thiosulfate-H2/CO2
Thiosulfate-Lactate
Sulfate-Lactate
ε WDirect (‰)
ε WCofa (‰)
ε SAS (‰)
ε SCofa (‰)
A
B
C
D
E
x=0
x=1
Heterotrophy
Min. lactate contribution to cofactors (s=0)
Max lactate contribution to cofactors (s=1)
Autotrophy
Min. H2 contribution to Ac-CoA (s=0)
Max. H2 contribution to Ac-CoA (s=1)

483

Figure 5. Isotope flux-balance model results for *Archaeoglobus fulgidus*. (A–C) Breakdown of the net isotope fractionation between lipid and water ($\varepsilon_{W,net}$; Fig. 4D–F) into two different isotope fractionation factors: $\varepsilon_{W,direct}$ for H atoms that are transferred through exchange during isomerization or addition via GGR, corresponding to $f_{W,direct}$ in Fig. 3, and $\varepsilon_{W,cofa}$ for H atoms that are transferred through cofactors (Fd_{red} and $F_{420}H_2$ for autotrophy, panel A; Fd_{red} for heterotrophy, panels B and C), corresponding to $f_{W,cofa}$ in Fig. 3. (D–E) Breakdown of the net isotope fractionation between lipid and substrate ($\varepsilon_{S,net}$; Fig. 4G–I) into two different isotope fractionation factors: $\varepsilon_{S,AS}$ for H atoms that are inherited directly from substrate via Ac-CoA, corresponding to $f_{S,AS}$ in Fig. 3, and $\varepsilon_{S,cofa}$ for H atoms that are transferred through cofactors (only applicable for heterotrophy via $F_{420}H_2$, panels D and E), corresponding to $f_{S,cofa}$ in Fig. 3. The lighter shaded areas refer to the s = 0 % (minimal substrate contribution) scenarios; darker shaded areas refer to the s = 100 % (maximal substrate contribution) scenarios. Solid lines and brown colors refer to heterotrophic conditions; dashed lines and purple colors refer to autotrophic conditions. See 4.2.1 and Table 3 for details of the conditions for each scenario.

5. Discussion

5.1. Effects of carbon metabolism and growth phase on lipid H isotopes composition in Archaea

The isotope flux-balance model results show a large fraction of lipid-H directly reflects water H isotope compositions, rather than substrate (lactate or H_2) isotope compositions in *A. fulgidus*. The $f_{W,net}$ is the net fraction of total biphytane H that directly records water H isotopes and is explicitly not derived from organic substrate or H_2. We observe larger $f_{W,net}$ for autotrophic growth ($f_{W,net}$ = 80–100 %), whereas $f_{W,net}$ for heterotrophic growth was lower ($f_{W,net}$ = 31–70 %; Table 3; Fig. 4A–C). Given that $\varepsilon_{W,net}$ is likely negative (i.e., a normal kinetic isotope fractionation), we can constrain the $f_{W,net}$ range that corresponds to $\varepsilon_{W,net} < 0$ (*see* Fig. 4D–E). This yields $f_{W,net}$ ranges of: 38–52 % for T-L and 42–52 % for S-L during exponential growth phase, versus 50–56 % for T-L and 52–54 % S-L during stationary growth phase. The lowest $f_{W,net}$ recorded were during heterotrophy in exponential phase, independent of the terminal electron acceptor. For stationary phase cultures of *A. fulgidus*, the $f_{W,net}$ was ≥80 % for autotrophy versus ≥50 % for heterotrophy. The $f_{W,net}$ range for lipids produced during stationary phase alone is likely larger, because lipids collected during stationary phase are a mixture of those produced during exponential phase and those newly produced during stationary phase. The higher $f_{W,net}$ range observed for autotrophy is reasonable, given that lactate is an additional source of H that contributes directly to Ac-CoA

synthesis during heterotrophy. A similar observation was reported for bacterial lipids where, for instance, the mole fraction of lipid H derived from water (≡ X_W in Zhang et al., 2009; herein equivalent to $f_{W,net}$) was larger for *Escherichia coli* grown on glucose compared to the same organism grown on complex medium (Zhang et al., 2009). Though the lipid synthesis pathways are different for Bacteria versus Archaea, it appears that the fractional contribution of substrates that are more direct precursors for lipid biosynthesis generally increases when organic substrates are used or H_2 is supplied in excess as an electron donor.

The effects of carbon metabolism and growth phase on lipid isotope composition have not been investigated in detail for archaeal lipids. Our results indicate that both the mode of metabolism and growth phase affect the lipid isotope composition (Table 3; Fig. 4). A recent study reported $\varepsilon_{L/W}$ of BPs produced by *N. maritimus* in continuous cultures at a range of doubling time and observed little change in $\varepsilon_{W/L}$ (0.18 ± 0.09 ‰ increase in $\varepsilon_{L/W}$ per hour increase in doubling time; Leavitt, Kopf et al., 2023). The relative variation in doubling time we observe for *A. fulgidus* grown on different substrates here in batch cultures (Table 2) is similar (*ca*. 3-fold variation) to the variation observed for *N. maritimus* in Leavitt, Kopf et al. (2023). A key difference here is that we do not strictly control growth and metabolic rates, as was the case for chemostat cultivation of *N. maritimus* (Leavitt, Kopf et al., 2023), and for *Sulfolobus acidocaldarius* (Harris et al., 2022). Nonetheless, the range of $\varepsilon_{L/W}$ we observe across different metabolic modes by *A. fulgidus* (–231 ± 6 ‰ for T-L, –241 ± 4 ‰ for S-L, and –271 ± 18 ‰ for T-H_2/CO_2; Table 2) is significant compared to the entire range of $\varepsilon_{L/W}$ observed across a similar variation in growth rate by *N. maritimus* (–272 ± 20 to –279 ± 8 ‰ for BP-0; Leavitt, Kopf et al., 2023). *N. maritimus* is an obligate chemoautotroph, such that all BP-bound H is strictly biosynthetic, whereas we show here

that patterns of $\varepsilon_{W/L}$ can change between heterotrophic and autotrophic growth conditions (Fig. 4 and Fig. 6). Our results support this hypothesis and show variation in $\varepsilon_{L/W}$ up to ~40 ‰ within the same metabolically versatile organism, in response to different electron donor-acceptor pairs and modes of carbon metabolism.

Even though the range of $\varepsilon_{L/W}$ in *A. fulgidus* is relatively larger compared to *N. maritimus*, the overall variation of $\varepsilon_{L/W}$ across all archaeal lipid studies to-date is consistently small compared to the variation observed across bacterial lipids (Fig. 6).

5.2. Factors that affect lipid-water H isotope fractionation across the three domains of life

Here we present a synthesis of the broader $\varepsilon_{L/W}$ patterns observed in lipids from all three domains of life. Archaeal lipids are characterized by a relatively narrow range of large and negative values of $\varepsilon_{L/W}$ across a wide range of organisms, metabolisms, and growth conditions (Fig. 6; Kaneko et al., 2011; Wu et al., 2020; Leavitt, Kopf et al., 2023; this study). This is in contrast with the domain Bacteria, where fatty acid $\varepsilon_{L/W}$ ranges a large span of >600 ‰ with both highly positive and negative values (Fig. 6; Campbell et al., 2009; Zhang et al., 2009; Dawson et al., 2015; Osburn et al., 2016; Wijker et al., 2019). Archaeal lipid $\varepsilon_{L/W}$ largely overlaps with that of eukaryotic lipid $\varepsilon_{L/W}$, although eukaryotic lipid $\varepsilon_{L/W}$ spans a significant range depending on the types of organism and classes of compound (Fig. 6; Sessions et al., 1999; Chikaraishi et al., 2004, 2009; Zhang and Sachs, 2007; Sachs et al., 2016). Notably, there are subgroups of both domains Bacteria and Eukarya that share similarities with Archaea in their $\varepsilon_{L/W}$. The shared similarities are interesting, given the difference in lipid biosynthesis mechanism among the three domains. Below, we take a closer look at the specific subsets of $\varepsilon_{L/W}$ values from the domains Euakrya and Bacteria that

resemble those from Archaea and discuss factors that may contribute to the large, negative values of $\varepsilon_{L/W}$ observed across the three domains.

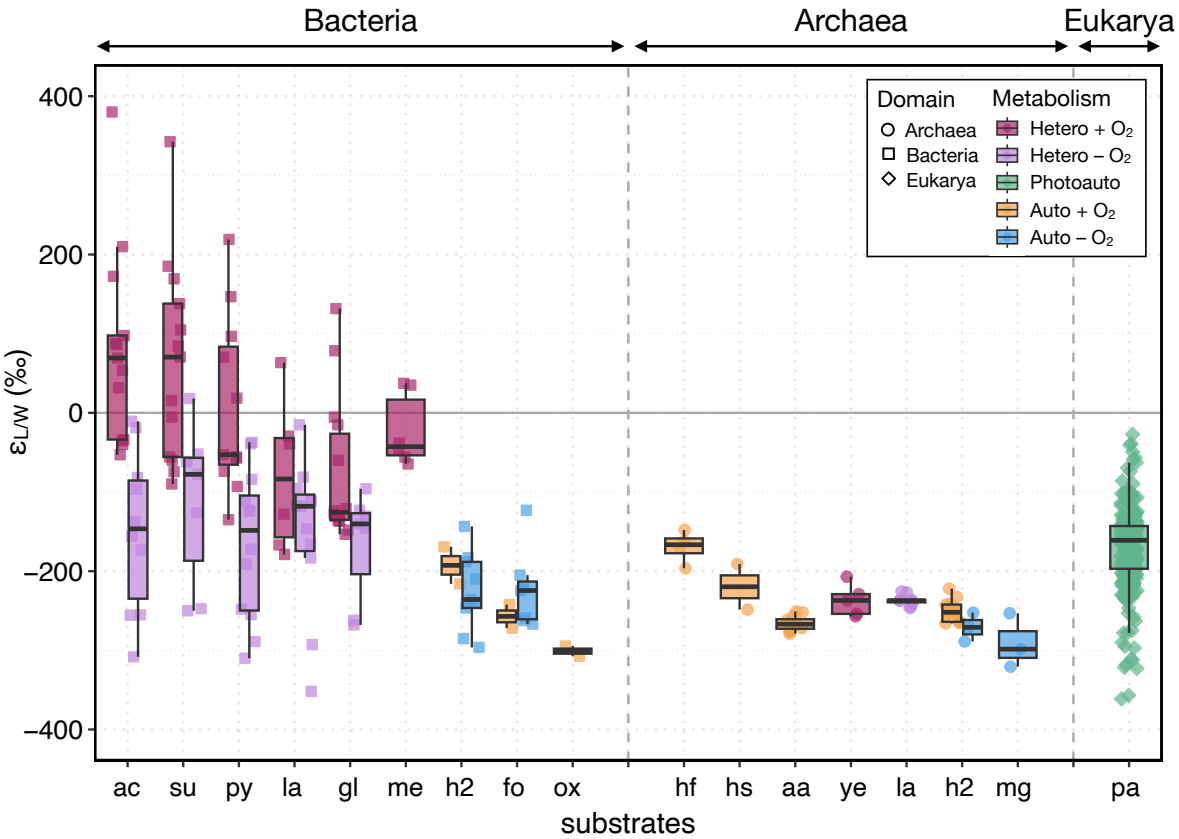

Figure 6. Summary of hydrogen isotope fractionation ($\varepsilon_{L/W}$) between lipids and water observed in culture studies. $\varepsilon_{L/W}$ values observed in all three domains of life: Archaea (circle), Bacteria (square), and Eukarya (diamond). Color codes represent different types of metabolism: aerobic heterotrophy (red), anaerobic heterotrophy (purple), oxygenic photoautotrophy (green), aerobic chemoautotrophy (orange), and anaerobic chemoautotrophy (blue). Electron donors used for biosynthesis are shown on the horizontal axis: acetate (ac); succinate (su); pyruvate (py); lactate (la); glucose (gl); methane (me); H_2+CO_2 (h2); formate (fo); oxalate (ox); H_2+Fe^{3+} (hf); H_2+S^0 (hs); ammonium (aa); yeast extract (ye); H_2, acetate or methanol for methanogenesis (mg); water for photoautotrophy (pa). Tested organisms for bacterial cultures include *C. oxalaticus*, *C. necator*, *R. palustris* (Zhang et al., 2009); *E. coli* (Zhang et al., 2009; Osburn et al., 2016; Wijker et al., 2019); *D. autotrophicum* (Campbell et al., 2009; Osburn et al., 2016); *M. capsulatus* (Sessions et al., 2002); *D. multivorans* (Dawson et al., 2015); *D. alaskensis* (Leavitt et al., 2016); *P. denitrificans*, *S. oneidensis*, *D. hydrogenophilus*, *D. alaskensis*, *D. propionicus* (Osburn et al., 2016); *B. subtilis*, *P. fluorescens*, *R. radiobacter*, and *E. meliloti* (Wijker et al., 2019). Tested organisms for eukaryotic cultures include *A. fundyense*, *I. galbana*, *Ascophyllum* sp., *F. vesiculosis*, *Z. marina*, *S. alterniflora* (Sessions et al., 1999); *C. japonica* (Chikaraishi et al., 2004); *B. braunii*, *E. unicocca*, *V. aureus* (Zhang and Sachs, 2007); *C. sativuc* (Chikaraishi et al., 2009); *E. huxleyi* (Sachs et al., 2016). Tested organisms for archaeal cultures include *Acidianus* sp. DS80 (this study); *N. maritimus* (Leavitt, Kopf et al., 2023); *Sulfolobus* sp. (Kaneko et al., 2011); *A. fulgidus* (this study); *Metallosphaera sedula* (this study); and *M. barkeri* (Wu et al., 2020).

5.2.1. Large lipid-water fractionation upon isoprenoid saturation in Archaea and Eukarya

The consistently large, negative values of $\varepsilon_{W/L}$ for archaeal lipids are notable considering the different types of organism and metabolic modes studied so far (Fig. 6). In Fig. 5, we present the model solution spaces for individual H fluxes, within either net flux that reflects water isotope composition (i.e., not affected by substrate contributions; $f_{W,net}$) or net flux that reflects isotopic contributions from organic substrate or H_2 ($f_{S,net}$), to further investigate specific parts of archaeal lipid biosynthesis pathway that may contribute to the observed large and negative values of $\varepsilon_{L/W}$. Prior work yielded estimates of $\alpha_W \cong 0.9$ for isotope fractionation associated with direct water incorporation across many bacteria (Zhang et al., 2009; Wijker et al., 2019), and $\varepsilon_{L/W}$ values modeled for *N. maritimus* with this empirical α_W were consistent with experimental observations (Leavitt, Kopf et al., 2023). Assuming an equivalent value of $\varepsilon_{W,direct}$ (i.e., isotope fractionation associated with the $f_{W,direct}$ flux is –100 ‰), we constrain plausible ranges of $\varepsilon_{W,cofa}$ in *A. fulgidus* (Fig. 5A–C). The ranges of $\varepsilon_{W,cofa}$ at $\varepsilon_{W,direct}$ = –100 ‰ are particularly well constrained for the autotrophic case (–599 to –436 ‰ at s = 0 %; –519 to –276 ‰ at s = 100 %; Fig. 5A).

It is plausible that both $\varepsilon_{W,cofa\text{-}AS}$ and $\varepsilon_{W,cofa\text{-}LS}$ have negative values that are comparable to the combined value of $\varepsilon_{W,cofa}$, as the less likely alternative would be a negative $\varepsilon_{W,cofa}$ that consists of very different $\varepsilon_{W,cofa\text{-}AS}$ and $\varepsilon_{W,cofa\text{-}LS}$. Our current model cannot distinguish between isotope fractionation factors associated with different fluxes within $f_{W,cofa}$ (i.e., $f_{W,cofa\text{-}AS}$ through Ac-CoA *vs*. $f_{W,cofa\text{-}LS}$ through NADPH), both of which can inherit H from cofactors $F_{420}H_2$ and/or Fd_{red} (Fig. 3B). However it is worth noting that, for both heterotrophic and autotrophic cases, a fraction of the $f_{W,cofa\text{-}LS}$ flux represents hydride transfer during the final saturation (double bond reduction) via GGR (Fig. 3; Step 10, Appendix B). Results of the isotope flux-balance model for *N. maritimus*

604 also indicated that the GGR reduction step is strongly fractionating (ε_{GGR} = –690 to –820 ‰ if
605 ε_{NADPH} = –100 to –300 ‰, depending on the degree of water exchange, or x_{ex} in this study),
606 regardless of how other model parameters are set (Leavitt, Kopf et al., 2023). Given how *N.*
607 *maritimus* and *A. fulgidus* share little in common otherwise (metabolically, genetically, and
608 biochemically), large fractionation associated with the GGR reduction step provides a
609 parsimonious explanation for the similar $\varepsilon_{L/W}$ values observed in the two organisms, as it is the
610 final step of archaeal lipid biosynthesis shared across all tetraether-producing Archaea. This would
611 be consistent with the similarly large, negative values of $\varepsilon_{L/W}$ observed in other archaeal lipids
612 (Fig. 6); testing more Archaea with the combined approach of isotope labeling experiments and
613 biochemically informed isotope flux-balance model will help further confirm this idea.
614
615 A closer examination of the eukaryotic lipids that share similar $\varepsilon_{L/W}$ values to archaeal lipids lends
616 further support to the notion that GGR reduction contributes to large H isotope fractionation
617 between lipids and water. Fig. 7A shows $\varepsilon_{L/W}$ for different subgroups of eukaryotic lipids,
618 categorized by three different biosynthetic pathways. In general, the two major families of lipids
619 are acetogenic and isoprenoid lipids which consist of acetate and isoprene monomeric units,
620 respectively (Pearson, 2014). Isoprenoid lipids are further divided into two groups, depending on
621 whether the isoprene (C_5) building blocks are synthesized via the mevalonic acid (MVA) pathway
622 (Lynen et al., 1958; Bloch, 1959) or the methylerythritol phosphate (MEP) pathway (Rohmer et
623 al., 1993). All Archaea discussed in this study synthesize isoprenoid lipids via the MVA pathway.
624 The MEP pathway is generally defined as bacterial and the MVA pathway as eukaryotic and
625 archaeal; both pathways often simultaneously occur in plants, where the MEP pathway is
626 expressed in chloroplasts (relics of the cyonobacterial plastid ancestor) and the MVA pathway is

627 expressed in the cytosol (Lichtenthaler et al., 1997; Lichtenthaler, 1999; Pearson, 2014). An
628 exception to this is the case of green algae, where both the cytosolic sterols and plastidic phytol
629 isoprenoids are synthesized via the MEP pathway (Lichtenthaler et al., 1997; Disch et al., 1998;
630 Pearson, 2014).
631
632 The three different biosynthetic pathways of eukaryotic lipids (acetogenic, MVA, and MEP) are
633 associated with distinct ranges of $\varepsilon_{L/W}$. In general, isoprenoid lipids have more negative $\varepsilon_{L/W}$
634 compared to acetogenic lipids (Estep and Hoering, 1980; Sessions et al., 1999). Among isoprenoid
635 lipids, plastidic isoprenoids such as phytols are more depleted in ^{2}H than the cytosolic counterparts
636 (Sessions et al., 1999; Chikaraishi et al., 2004, 2009). This general trend is captured in Fig. 7A,
637 where acetogenic lipids (e.g., *n*-alkanol and *n*-alkyl lipids including fatty acids) have more positive
638 $\varepsilon_{L/W}$ compared to isoprenoid lipids. The C_{15} and C_{30} isoprenoids synthesized via the MVA pathway
639 (e.g., sterol, triterpenoids, sesquiterpenes, squalene) are relatively more enriched in ^{2}H compared
640 to the C_{20} isoprenoids (e.g., phytol, phytadiene, diterpenes) and botryococcenes (triterpenes)
641 synthesized via the MEP pathway (Fig. 7A).
642
643 While the relative difference in $\varepsilon_{L/W}$ between MVA and MEP pathways holds in general, the larger
644 and more negative values of $\varepsilon_{L/W}$ appear to correlate more with highly fractionating enzymatic
645 steps, rather than specific pathways. For example, Chikaraishi et al. (2004) observed in
646 *Cryptomeria japonica* (conifer) that $\varepsilon_{L/W}$ values for cytosolic lipids produced via the MVA
647 pathway, sesquiterpenes (–228 to –238 ‰) and squalene (–225 to –251 ‰), are similar to those
648 for plastidic diterpenoids (–238 to –251 ‰) produced via the MEP pathway (Fig. 7A). Phytol and
649 botryococcenes, on the other hand, have particularly negative $\varepsilon_{L/W}$ values among eukaryotic lipids

produced via the MEP pathway. For example, Zhang and Sachs (2007) found that botryococcenes with longer chain lengths had progressively lower δ^2H compared to the C_{30} botryococcene (precursor to all other botryococcenes) in *Botryococcus braunii* race B. They hypothesized that significantly ^{2}H-depleted hydrogen from methionine is incorporated into botryococcene during the step-wise methylation (Zhang and Sachs, 2007). Similarly, phytol in *C. japonica* had up to 65 ‰ more negative $\varepsilon_{L/W}$ compared to diterpenoids, another plastidic lipid produced via the MEP pathway within the same organism (Chikaraishi et al., 2004). Later, Chikaraishi et al. (2009) observed a gradual depletion in δ^2H from phytol precursors (starting from geranylgeraniol) to phytol in cucumber, indicating that significantly ^{2}H-depleted hydrogen is incorporated into phytol and its precursors during the step-wise hydrogenation catalyzed by GGR ($\varepsilon_{GGR} \cong -650$ ‰; Chikaraishi et al., 2009).

The $\varepsilon_{L/W}$ values of phytol (and its dehydration product phytadiene) investigated in a wide range of eukaryotes so far are all significantly large and negative (e.g., –357 to –278 ‰ for phytol in dinoflagellate, coccolithophore, marsh grass, cucumber, and conifer; Fig. 7A). Similarly, all values of $\varepsilon_{L/W}$ investigated in a range of different archaea are significantly large and negative (e.g., –341 to –148 ‰ for phytanes and biphytanes in *N. maritimus*, *Sulfolobus* sp., *M. sedula*, *Acidianus* sp., *M. barkeri*, and *A. fulgidus*; Fig. 7A). Taken together, empirical and model-based results suggest that the GGR reduction is a highly fractionating step that contribute to the large fractionation observed in both eukaryotic and archaeal lipid synthesis (Chikaraishi et al., 2009; Leavitt, Kopf et al., 2023; this study, Fig. 5 and Fig. 6).

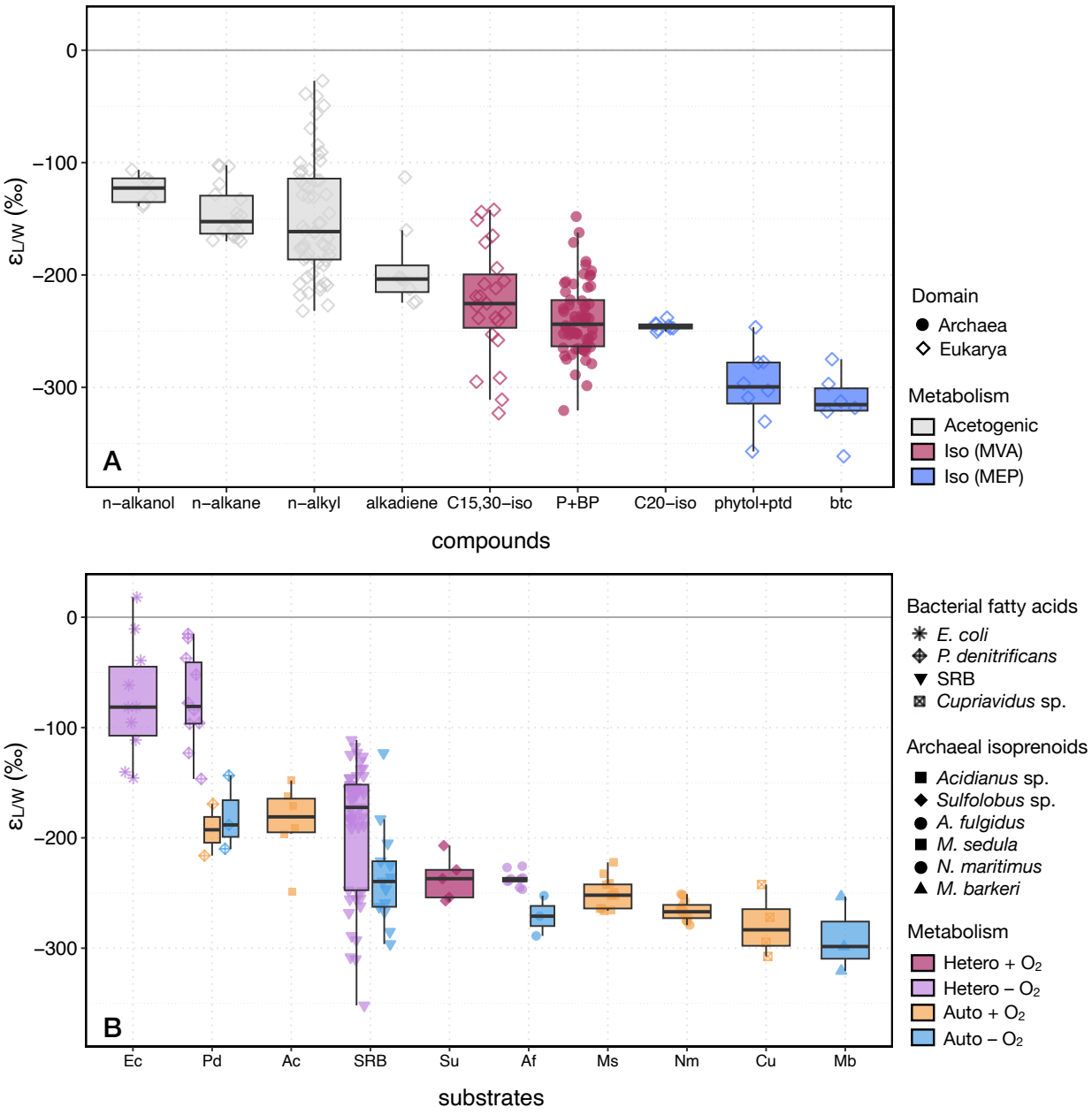
0
−100
−200
−300
εL/W (‰)
A
n−alkanol
n−alkane
n−alkyl
alkadiene
C15,30−iso
P+BP
C20−iso
phytol+ptd
btc
compounds
Domain
Archaea
Eukarya
Metabolism
Acetogenic
Iso (MVA)
Iso (MEP)
B
Ec
Pd
Ac
SRB
Su
Af
Ms
Nm
Cu
Mb
substrates
Bacterial fatty acids
E. coli
P. denitrificans
SRB
Cupriavidus sp.
Archaeal isoprenoids
Acidianus sp.
Sulfolobus sp.
A. fulgidus
M. sedula
N. maritimus
M. barkeri
Metabolism
Hetero + O2
Hetero − O2
Auto + O2
Auto − O2

672

Figure 7. Comparison of $\varepsilon_{L/W}$ values observed in eukaryotic *vs*. archaeal lipids and in bacterial *vs*. archaeal lipids. **(A)** $\varepsilon_{L/W}$ values observed in acetogenic and isoprenoid lipids from the domains Archaea and Eukarya. Different classes of compounds are shown on the horizontal axis. Compounds shown for acetogenic pathway: n-alkanol, *n*-alkane, *n*-alkyl (*n*-alkanoic acids and fatty acids), and alkadiene. For the MVA pathway: C_{15} and C_{30} isoprenoids (sterol, squalene, triterpenoids, and sesquiterpenes) and P+BP (phytanes and biphytanes). For the MEP pathway: C_{20} isoprenoids (diterpenes, sandaracopimarinol, ferruginol, diterpenol, and sugiol), phytol+ptd (phytol and phytadiene), and btc (botryococcene). **(B)** $\varepsilon_{L/W}$ values observed in fatty acids from anaerobic and/or autotrophic Bacteria and isoprenoid lipids from Archaea. Different organisms are shown on the horizontal axis. For Bacteria: *E. coli* (Ec), *Paracoccus denitrificans* (Pd), SRB (*Desulfobacterium autotrophicum*, *Desulfococcus multivorans*, *Desulfobacter hydrogenophilus*, *Desulfovibrio alaskensis*, *Desulfolobus propionicus*), and *Cupriavidus* sp. (Cu). For Archaea: *Acidianus* sp. DS80 (Ac), *Sulfolobus* sp. (Su), *Archaeoglobus fulgidus* (Af), *Metallosphaera sedula* (Ms), *Nitrosopumilus maritimus* (Nm), and *Methanosarcina barkeri* (Mb). A full list of references can be found in Appendix C.

5.2.2. Energy limitation and lipid-water fractionation in Archaeal versus Bacterial lipids

Besides the shared biochemical mechanism underlying negative $\varepsilon_{L/W}$ in eukaryotic and archaeal lipids, another interesting pattern emerges from comparison of $\varepsilon_{L/W}$ across the three domains of life: a subset of bacterial lipids resembles archaeal lipids in its consistently negative $\varepsilon_{L/W}$ values (Fig. 6). For bacterial lipids, anaerobiosis and/or autotrophy appear to be associated with consistently large, negative values of $\varepsilon_{L/W}$. Examples include aerobic autotrophy (*Cupriavidus oxalaticus*, Zhang et al., 2009; *Paracoccus denitrificans*, Osburn et al., 2016), anaerobic autotrophy (*Desulfobacterium autotrophicum*, Campbell et al., 2009; *Desulfococcus multivorans*, Dawson et al., 2015; *P. denitrificans*, *Desulfobacterium autotrophicum*, *Desulfovibrio alaskensis*, Osburn et al., 2016), and anaerobic heterotrophy (*D. multivorans*, Dawson et al., 2015; *P. denitrificans*, *Escherichia coli*, *D. autotrophicum*, *Desulfobacter hydrogenophilus*, *D. alaskensis*, *Desulfolobus propionicus*, Osburn et al., 2016) (Fig. 6; Fig. 7B). Of these modes of metabolism, aerobic or anaerobic autotrophy has a more constrained range of $\varepsilon_{W/L}$ and more overlaps with $\varepsilon_{L/W}$ observed in archaeal lipids, compared to anaerobic heterotrophy (Fig. 6; Fig. 7B). We propose that NADPH flux imbalances associated with energy limitation that broadly characterize autotrophic and/or anaerobic modes of metabolism contribute to the apparent similarity in $\varepsilon_{L/W}$ observed between the domains of Bacteria and Archaea.

703

704 The concept of NADPH flux imbalance set forth by Wijker et al. (2019) provides a quantitative
705 framework to relate metabolism-dependent patterns of $\varepsilon_{L/W}$ observed in aerobic heterotrophs to the
706 fluxes of H through specific dehydrogenase and transhydrogenase enzymes. For the highly
707 conserved fatty acid biosynthesis pathway, NADPH serves as the reducing agent for the reduction
708 of acyl intermediates (Wakil et al., 1983). As a result, NADPH accounts for ~50% of fatty acid H
709 (Sessions et al., 1999). Wijker et al. (2019) showed that $\varepsilon_{L/W}$ values of fatty acids produced by five
710 wild-type species of aerobic heterotrophic bacteria are positively correlated with relative NADPH
711 imbalance flux. Among the tested aerobic heterotrophs, two species (*E. coli* and *B. subtilis*) had
712 moderately negative values of NADPH flux imbalance (–32 and –11 %, respectively) (Wijker et
713 al., 2019). Here, negative values reflect underproduction of NADPH where catabolic production
714 of NADPH does not meet the anabolic requirement (Wijker et al., 2019). Furthermore, the results
715 from *E. coli* knockout mutants confirmed the direction of isotope fractionation for specific
716 transhydrogenases (e.g., ^{2}H-depletion by NADPH-producing PntAB and ^{2}H-enrichment by
717 NADPH-consuming UDhA) (Wijker et al., 2019).

718

719 For microbes adapted to chronic energy limitation, even more negative values of NADPH flux
720 imbalance would be expected where just enough NADPH is produced such that most to all of it is
721 used for biosynthesis (i.e., little to no flux from NADPH back to NADH). This prediction is
722 consistent with the general concept of energy spilling (also known as growth uncoupling or
723 overflow metabolism), which suggests that microbes under energy limitation tend to have more
724 efficient biomass production (Russell, 2007). For example, *E. coli* grown aerobically resulted in
725 more than 9-fold increase in ATP production per mole of glucose compared to the anaerobic

726 counterpart; however, the biomass yield was only 2-fold greater during aerobic respiration
727 (Stouthamer and Bettenhaussen, 1977; Gottschalk, 1986). Similar phenomenon of energy spilling
728 has also been observed in methanogenic archaea. For example, *Methanothermobacter*
729 *thermautotrophicus* and *Methanococcus maripaludis* produced less biomass per mole of methane
730 when H_2 (electron donor) was present in excess compared to H_2-limiting condition (Morgan et al.,
731 1997; De Poorter et al., 2007; Costa et al., 2013).
732
733 In line with the observed and expected outcomes of energy limitation (negative NADPH flux
734 imbalance and tighter coupling between catabolism and anabolism), Leavitt, Kopf et al. (2023)
735 found that $\varepsilon_{L/W}$ values for *N. maritimus* fall within the 95% confidence interval for the extension
736 of Wijker et al. (2019) regression when an extremely negative value (–100 %) of NADPH flux
737 imbalance was assigned. The apparent fit of *N. maritimus* $\varepsilon_{L/W}$ on the negative end of the
738 framework is reasonable, given that *N. maritimus* is an obligate autotroph adapted to oligotrophic
739 nitrification with energy-efficient CO_2 fixation pathway (Martens-Habbena et al., 2009; Könneke
740 et al., 2014). The fact that all archaeal lipids investigated for $\varepsilon_{L/W}$ so far fall within a relatively
741 narrow range of negative values (Fig. 6; Fig. 7B) may, at least partially, reflect the general concept
742 that Archaea are optimized for chronic energy limitation (Valentine, 2007). The results from this
743 study show that, while metabolic modes and growth rates have significant impacts on $\varepsilon_{L/W}$ within
744 a single organism (*A. fulgidus*), the observed variation in $\varepsilon_{L/W}$ still falls within the overall range
745 observed across archaeal lipids (e.g., heterotrophic and autotrophic *A. fulgidus* 'Af' data *vs*. other
746 archaeal lipids data; Fig. 7B).
747

748 The similarity between archaeal lipids and a subset of anaerobic and/or autotrophic bacterial lipids
749 is striking (Fig. 6; Fig. 7B) given the fundamental differences in fatty acid and isoprenoid lipid
750 biosynthesis pathways. This suggests that factors controlling microbial $\varepsilon_{L/W}$ may not be domain-
751 specific; instead, common challenges associated with anaerobic respiration and/or autotrophy (i.e.,
752 lower free energy yields and/or additional energetic costs for CO_2 fixation) may become primary
753 controlling factors of $\varepsilon_{L/W}$ for both Bacteria and Archaea. Notably, the range of $\varepsilon_{L/W}$ in fatty acids
754 produced by sulfate-reducing bacteria (SRB) is much narrower compared to that observed in
755 aerobic heterotrophs regardless of metabolic pathway or substrate (Fig. 7B).
756
757 One of the transhydrogenases that plays an important role in SRB is NfnAB, and it has been shown
758 that this enzyme is important for H isotope fractionation in *D. alaskensis* (Leavitt et al., 2016). The
759 details of the magnitude of $\varepsilon_{L/W}$ set by NfnAB under severe NADPH underproduction may be
760 complicated by other processes such as intracellular isotope distillation (i.e., more quantitative
761 transfer of NADPH hydride to lipids) as suggested by Leavitt et al. (2016). Regardless, given that
762 decoupling of NADPH production for anabolism from NADH for catabolism becomes more
763 important during energy limitation, transhydrogenases that are widely distributed among anaerobic
764 bacteria (namely NfnAB; Pereira et al., 2011; Leavitt et al., 2016; Buckel and Thauer, 2018) may
765 be key contributing factors for the negative $\varepsilon_{W/L}$ observed across these organisms (Fig. 6; Fig. 7B).
766 It is worth noting that *nfnAB* was not found in archaeal species investigated by Pereira et al. (2011),
767 including *A. fulgidus*.
768
769 A complex interplay among environmental, physiological, and enzymatic factors underlies net
770 isotope fractionation patterns observed in a biosynthetic product such as $\varepsilon_{L/W}$. For archaeal lipids

and a subset of bacterial lipids, however, two factors appear to play key roles in shaping the consistently negative $\varepsilon_{L/W}$ patterns observed in the lipids from both domains: highly fractionating enzymatic steps (e.g., GGR in archaeal isoprenoid lipid biosynthesis; transhydrogenases in bacterial fatty acid biosynthesis) and energy limitation (i.e., NADPH flux imbalance). The negative $\varepsilon_{L/W}$ commonly observed in archaea and a subset of bacteria is likely a convergent feature resulting from a combination of both factors. A better mechanistic understanding of factors conducive to similar patterns of $\varepsilon_{L/W}$ in bacterial and archaeal lipids could lead to biogeochemical and/or ecological insights that are unique to microbial life. This would, in turn, significantly expand the application of lipid biomarkers as paleoenvironmental or paleoecological proxy currently possible with eukaryotic or bacterial lipids alone.

6. Conclusion

In this study, we conducted water isotope label experiments with a metabolically flexible and well-studied model archaeon *A. fulgidus* and quantified the hydrogen isotope fractionation between lipids and water in response to different carbon substrates and electron donor-acceptor pairs. We observed changes in regression parameters among experimental conditions, where higher slopes ($f_W \cdot {}^2\alpha_{L/W}$) were observed in autotrophic compared to heterotrophic conditions and during stationary compared to exponential growth phase. The bio-isotopic model further constrains individual parameters such as fluxes that reflect water isotope composition (i.e., not affected by substrate isotope composition) (f_W) and isotope fractionation between lipids and water ($\varepsilon_{L/W}$) that together make up the slope. These results are consistent with observations from regression parameters, where f_W is larger under autotrophic condition and during stationary growth phase compared to the heterotrophic conditions and exponential growth phase. The model results also

allow us to constrain plausible ranges of isotope fractionation associated with a specific route of hydrogen flux (e.g., flux for direct water incorporation *vs*. flux from water through cofactors). The model results point toward the isotope fractionation associated with the $f_{W,cofa}$ flux, which includes the hydride transfer during the final saturation via GGR, as a highly fractionating step. This is consistent with recent bio-isotopic model results for another archaeon *N. maritimus*. Finally, we synthesized a three-domain comparison of $\varepsilon_{L/W}$ patterns which suggests that the highly fractionating double bond reduction via GGR may also explain the similarly large and negative values of $\varepsilon_{L/W}$ observed between eukaryotic and archaeal lipids. Furthermore, the shared negative $\varepsilon_{L/W}$ values between fatty acids in anaerobic and/or autotrophic bacteria and isoprenoids in archaea may be associated with the general state of energy limitation experienced by the different groups of organisms. Additional experimental work with archaea that use carbon metabolism pathways that have not been examined with the bio-isotopic model (i.e., 3HP/4HB and reductive Wood-Ljungdahl pathways) as well as more systematic comparisons between bacterial and archaeal lipids will help determine the scope of applicability for microbial lipid $\varepsilon_{L/W}$ in paleoenvironmental and paleoecological studies.

7. Data availability

Access to all data products and code for the isotope flux-balance model for this manuscript are available at: https://github.com/jrhim/Rhim_et_al_2024_GCA.

8. CRediT authorship contribution statement

Jeemin H. Rhim: Conceptualization, Methodology, Investigation, Data Curation, Writing – Original Draft, Writing – Review & Editing, Visualization. **Sebastian Kopf:** Conceptualization,

Methodology, Resources, Writing – Review & Editing, Supervision, Funding acquisition. **Jamie McFarlin:** Investigation, Writing – Review & Editing. **Ashley E. Maloney:** Investigation, Writing – Review & Editing. **Harpreet Batther:** Investigation, Writing – Review & Editing. **Carolynn M. Harris:** Investigation, Writing – Review & Editing. **Alice Zhou:** Investigation, Writing – Review & Editing. **Xiahong Feng:** Investigation, Writing – Review & Editing. **Yuki Weber:** Investigation, Writing – Review & Editing. **Shelley Hoeft-McCann:** Investigation, Writing – Review & Editing. **Ann Pearson:** Resources, Writing – Review & Editing, Supervision, Funding acquisition. **William D. Leavitt:** Conceptualization, Resources, Writing – Review & Editing, Supervision, Funding acquisition.

9. Declaration of competing interest

The authors declare that they have no known competing financial interests or personal relationships that could have appeared to influence the work reported in this paper.

10. Acknowledgements

This research was supported by funding from: collaborative research grant NSF EAR #1928303 (WDL, SHK); the American Chemical Society PRF #57209-DNI2 (WDL, YW); Simons Foundation Award #623881 (WDL); Swiss National Science Foundation P2BSP2_168716 (YW); NSF OCE-1843285 and 1702262 (AP). JHR was supported by the Dartmouth College Society of Fellows. We thank Ashley Maloney (CU Boulder), Felix Elling (then at Harvard), and Beverly Chiu (then at Dartmouth) for expert laboratory assistance.

11. Appendix A. Supplementary material

These include the Overview of hydrogen budget, Culturing conditions for *Acidianus* sp. and *Metallosphaera sedula*, Full list of references for Figure 7, and Supplemental Figures 1–2.

12. References

Achenbach-Richter L., Stetter K. O. and Woese C. R. (1987) A possible biochemical missing link among archaebacteria. *Nature* **327**, 348–349.

Bender A. L. D. (2017) Genetic and Biological Studies on Solanum Plants: Insights into the Leaf Wax Alkane Paleoclimate Proxy.

Bloch K. (1959) Biogenesis and transformations of squalene. In *Biosynthesis of Terpenes and Sterols* Little, Brown and Company.

Boyd E. S., Jackson R. A., Encarnacion G., Zahn J. A., Beard T., Leavitt W. D., Pi Y., Zhang C. L., Pearson A. and Geesey G. G. (2007) Isolation, Characterization, and Ecology of Sulfur-Respiring *Crenarchaea* Inhabiting Acid-Sulfate-Chloride-Containing Geothermal Springs in Yellowstone National Park. *Appl. Environ. Microbiol.* **73**, 6669–6677.

Brock T. D., Brock K. M., Belly R. T. and Weiss R. L. (1972) Sulfolobus: A new genus of sulfur-oxidizing bacteria living at low pH and high temperature. *Arch. F□r Mikrobiol.* **84**, 54–68.

Buckel W. and Thauer R. K. (2018) Flavin-Based Electron Bifurcation, Ferredoxin, Flavodoxin, and Anaerobic Respiration With Protons (Ech) or NAD+ (Rnf) as Electron Acceptors: A Historical Review. *Front. Microbiol.* **9**, 401.

Campbell B. J., Li C., Sessions A. L. and Valentine D. L. (2009) Hydrogen isotopic fractionation in lipid biosynthesis by H2-consuming Desulfobacterium autotrophicum. *Geochim. Cosmochim. Acta* **73**, 2744–2757.

Chikaraishi Y. and Naraoka H. (2003) Compound-specific δD–δ13C analyses of n-alkanes extracted from terrestrial and aquatic plants. *Phytochemistry* **63**, 361–371.

Chikaraishi Y., Naraoka H. and Poulson S. R. (2004) Carbon and hydrogen isotopic fractionation during lipid biosynthesis in a higher plant (Cryptomeria japonica). *Phytochemistry* **65**, 323–330.

Chikaraishi Y., Tanaka R., Tanaka A. and Ohkouchi N. (2009) Fractionation of hydrogen isotopes during phytol biosynthesis. *Org. Geochem.* **40**, 569–573.

Costa K. C., Yoon S. H., Pan M., Burn J. A., Baliga N. S. and Leigh J. A. (2013) Effects of H_2 and Formate on Growth Yield and Regulation of Methanogenesis in Methanococcus maripaludis. *J. Bacteriol.* **195**, 1456–1462.

Dawson K. S., Osburn M. R., Sessions A. L. and Orphan V. J. (2015) Metabolic associations with archaea drive shifts in hydrogen isotope fractionation in sulfate-reducing bacterial lipids in cocultures and methane seeps. *Geobiology* **13**, 462–477.

De Poorter L. M. I., Geerts W. J. and Keltjens J. T. (2007) Coupling of *Methanothermobacter thermautotrophicus* Methane Formation and Growth in Fed-Batch and Continuous Cultures under Different H_2 Gassing Regimens. *Appl. Environ. Microbiol.* **73**, 740–749.

Dirghangi S. S. and Pagani M. (2013) Hydrogen isotope fractionation during lipid biosynthesis by Haloarcula marismortui. *Geochim. Cosmochim. Acta* **119**, 381–390.

Disch A., Schwender J., Müller C., Lichtenthaler H. K. and Rohmer M. (1998) Distribution of the mevalonate and glyceraldehyde phosphate/pyruvate pathways for isoprenoid biosynthesis in unicellular algae and the cyanobacterium Synechocystis PCC 6714. *Biochem. J.* **333**, 381–388.

Estep M. F. and Hoering T. C. (1980) Biogeochemistry of the stable hydrogen isotopes. *Geochim. Cosmochim. Acta* **44**, 1197–1206.

Gottschalk (1986) Regulation of Bacterial Metabolism.

Harris C., Rhim J., Zhang Y., Cobban A., McFarlin J., Batther H., Kopf S. and Leavitt W. (2022) Determining controls on hydrogen isotope fractionation in archaeal tetraether lipids in a thermoacidophilic archaeal heterotroph. In *Goldschmidt2022 abstracts* Goldschmidt2022. European Association of Geochemistry, Honolulu, HI, USA.

Hayes J. M. (2001) Fractionation of the Isotopes of Carbon and Hydrogen in Biosynthetic Processes. *Stable Isot. Geochem.*, 225–277.

Hendrickson E. L. and Leigh J. A. (2008) Roles of Coenzyme F_{420} -Reducing Hydrogenases and Hydrogen- and F_{420} -Dependent Methylenetetrahydromethanopterin Dehydrogenases in Reduction of F_{420} and Production of Hydrogen during Methanogenesis. *J. Bacteriol.* **190**, 4818–4821.

Hocking W. P., Stokke R., Roalkvam I. and Steen I. H. (2014) Identification of key components in the energy metabolism of the hyperthermophilic sulfate-reducing archaeon Archaeoglobus fulgidus by transcriptome analyses. *Front. Microbiol.* **5**.

Kaneko M., Kitajima F. and Naraoka H. (2011) Stable hydrogen isotope measurement of archaeal ether-bound hydrocarbons. *Org. Geochem.* **42**, 166–172.

Klein A. R., Breitung J., Linger D., Stetter K. O. and Thauer R. K. (1993) extremely thermophilic sulfate reducing Archaeoglobusfulgidus: comparison of its properties with those of the cyclohydrolase from the extremely thermophilic Methanopyrus kandleri.

Könneke M., Schubert D. M., Brown P. C., Hügler M., Standfest S., Schwander T., Schada Von Borzyskowski L., Erb T. J., Stahl D. A. and Berg I. A. (2014) Ammonia-oxidizing archaea use the most energy-efficient aerobic pathway for CO_2 fixation. *Proc. Natl. Acad. Sci.* **111**, 8239–8244.

Kopec B. G., Feng X., Posmentier E. S. and Sonder L. J. (2019) Seasonal Deuterium Excess Variations of Precipitation at Summit, Greenland, and their Climatological Significance. *J. Geophys. Res. Atmospheres* **124**, 72–91.

Kopf S., Davidheiser-Kroll B. and Kocken I. (2021) Isoreader: An R package to read stable isotope data files for reproducible research. *J. Open Source Softw.* **6**, 2878.

Kunow J., Schwörer B., Stetter K. O. and Thauer R. K. (1993) A F420-dependent NADP reductase in the extremely thermophilie sulfate-reducing Archaeoglobusfulgidus.

Ladd S. N. and Sachs J. P. (2017) 2H/1H fractionation in lipids of the mangrove Bruguiera gymnorhiza increases with salinity in marine lakes of Palau. *Geochim. Cosmochim. Acta* **204**, 300–312.

Lai D., Springstead J. R. and Monbouquette H. G. (2008) Effect of growth temperature on ether lipid biochemistry in Archaeoglobus fulgidus. *Extremophiles* **12**, 271–278.

Leavitt W. D., Kopf S. H., Weber Y., Chiu B., McFarlin J. M., Elling F. J., Hoeft-McCann S. and Pearson A. (2023) Controls on the hydrogen isotope composition of tetraether lipids in an autotrophic ammonia-oxidizing marine archaeon. *Geochim. Cosmochim. Acta* **352**, 194–210.

Leavitt W. D., Venceslau S. S., Pereira I. A. C., Johnston D. T. and Bradley A. S. (2016) Fractionation of sulfur and hydrogen isotopes in *Desulfovibrio vulgaris* with perturbed DsrC expression ed. R. Boden. *FEMS Microbiol. Lett.* **363**, fnw226.

Lengger S. K., Weber Y., Taylor K. W. R., Kopf S. H., Berstan R., Bull I. D., Mayser J., Leavitt W. D., Blewett J., Pearson A. and Pancost R. D. (2021) Determination of the δ^2H values of high molecular weight lipids by high-temperature gas chromatography coupled to isotope ratio mass spectrometry. *Rapid Commun. Mass Spectrom.* **35**, e8983.

Lichtenthaler H. K. (1999) THE 1-DEOXY-D-XYLULOSE-5-PHOSPHATE PATHWAY OF ISOPRENOID BIOSYNTHESIS IN PLANTS. *Annu. Rev. Plant Physiol. Plant Mol. Biol.* **50**, 47–65.

Lichtenthaler H. K., Rohmer M. and Schwender J. (1997) Two independent biochemical pathways for isopentenyl diphosphate and isoprenoid biosynthesis in higher plants. *Physiol. Plant.* **101**, 643–652.

Lynen F., Eggerer H., Henning U. and Kessel I. (1958) Farnesyl-pyrophosphat und 3-Methyl-Δ^3-butenyl-1-pyrophosphat, die biologischen Vorstufen des Squalens. Zur Biosynthese der Terpene, III. *Angew. Chem.* **70**, 738–742.

Maloney A. E., Shinneman A. L. C., Hemeon K. and Sachs J. P. (2016) Exploring lipid 2H/1H fractionation mechanisms in response to salinity with continuous cultures of the diatom Thalassiosira pseudonana. *Org. Geochem.* **101**, 154–165.

Martens-Habbena W., Berube P. M., Urakawa H., De La Torre J. R. and Stahl D. A. (2009) Ammonia oxidation kinetics determine niche separation of nitrifying Archaea and Bacteria. *Nature* **461**, 976–979.

McFarlin J. M., Axford Y., Masterson A. L. and Osburn M. R. (2019) Calibration of modern sedimentary δ2H plant wax-water relationships in Greenland lakes. *Quat. Sci. Rev.* **225**, 105978.

Möller-Zinkhan D., Börner G. and Thauer R. K. (1989) Function of methanofuran, tetrahydromethanopterin, and coenzyme F42oin Archaeoglobusfulgidus.

Möller-Zinkhan D. and Thauer R. K. (1990) Anaerobic lactate oxidation to 3 CO2 by Archaeoglobus fulgidus via the carbon monoxide dehydrogenase pathway: demonstration of the acetyl-CoA carbon-carbon cleavage reaction in cell extracts. *Arch. Microbiol.* **153**, 215–218.

Morgan R. M., Pihl T. D., Lling J. R. N. and Reeve J. N. (1997) Hydrogen Regulation of Growth, Growth Yields, and Methane Gene Transcription in Methanobacterium thermoautotrophicum ⌬H. *J BACTERIOL* **179**.

Osburn M. R., Dawson K. S., Fogel M. L. and Sessions A. L. (2016) Fractionation of Hydrogen Isotopes by Sulfate- and Nitrate-Reducing Bacteria. *Front. Microbiol.* **7**.

Pearson A. (2014) Lipidomics for Geochemistry. In *Treatise on Geochemistry* Elsevier. pp. 291–336.

Pereira I. A. C., Ramos A. R., Grein F., Marques M. C., Da Silva S. M. and Venceslau S. S. (2011) A Comparative Genomic Analysis of Energy Metabolism in Sulfate Reducing Bacteria and Archaea. *Front. Microbiol.* **2**.

Reed D. W. and Hartzell P. L. (1999) The Archaeoglobus fulgidus D-Lactate Dehydrogenase Is a Zn2Ƣ Flavoprotein. *J BACTERIOL* **181**.

Rhim J. H., Zhou A., Amenabar M. J., Boyer G. M., Elling F. J., Weber Y., Pearson A., Boyd E. S. and Leavitt W. D. (2024) Mode of carbon and energy metabolism shifts lipid composition in the thermoacidophile *Acidianus* ed. J. R. Spear. *Appl. Environ. Microbiol.*, e01369-23.

Rohmer M., Knani M., Simonin P., Sutter B. and Sahm H. (1993) Isoprenoid biosynthesis in bacteria: a novel pathway for the early steps leading to isopentenyl diphosphate. *Biochem. J.* **295**, 517–524.

Russell J. B. (2007) The Energy Spilling Reactions of Bacteria and Other Organisms. *Microb. Physiol.* **13**, 1–11.

Sachs J. P. (2014) Hydrogen Isotope Signatures in the Lipids of Phytoplankton. In *Treatise on Geochemistry* Elsevier. pp. 79–94.

Sachs J. P. and Kawka O. E. (2015) The Influence of Growth Rate on 2H/1H Fractionation in Continuous Cultures of the Coccolithophorid Emiliania huxleyi and the Diatom Thalassiosira pseudonana ed. G. P. Tochtrop. *PLOS ONE* **10**, e0141643.

Sachs J. P., Maloney A. E. and Gregersen J. (2017) Effect of light on 2H/1H fractionation in lipids from continuous cultures of the diatom Thalassiosira pseudonana. *Geochim. Cosmochim. Acta* **209**, 204–215.

Sachs J. P., Maloney A. E., Gregersen J. and Paschall C. (2016) Effect of salinity on 2H/1H fractionation in lipids from continuous cultures of the coccolithophorid Emiliania huxleyi. *Geochim. Cosmochim. Acta* **189**, 96–109.

Sachse D., Billault I., Bowen G. J., Chikaraishi Y., Dawson T. E., Feakins S. J., Freeman K. H., Magill C. R., McInerney F. A., van der Meer M. T. J., Polissar P., Robins R. J., Sachs J. P., Schmidt H.-L., Sessions A. L., White J. W. C., West J. B. and Kahmen A. (2012) Molecular Paleohydrology: Interpreting the Hydrogen-Isotopic Composition of Lipid Biomarkers from Photosynthesizing Organisms. *Annu. Rev. Earth Planet. Sci.* **40**, 221–249.

Schmitz R. A., Linder D., Stetter K. O. and Thauer R. K. (1991) N s,N1~ reductase (coenzyme F42o-dependent) and formylmethanofurandehydrogenase from the hyperthermophileArchaeoglobusfulgidus.

Schwörer B., Breitung J., Klein A. R., Stetter K. O. and Thauer R. K. (1993) Formylmethanofuran: tetrahydromethanopterin formyltransferase and NS,N ~ dehydrogenase from the sulfate-reducing Archaeoglobusfulgidus: similarities with the enzymes from methanogenic Archaea.

Sessions A. L. (2016) Factors controlling the deuterium contents of sedimentary hydrocarbons. *Org. Geochem.* **96**, 43–64.

Sessions A. L., Burgoyne T. W., Schimmelmann A. and Hayes J. M. (1999) Fractionation of hydrogen isotopes in lipid biosynthesis. *Org. Geochem.* **30**, 1193–1200.

Sessions A. L., Jahnke L. L., Schimmelmann A. and Hayes J. M. (2002) Hydrogen isotope fractionation in lipids of the methane-oxidizing bacterium Methylococcus capsulatus. *Geochim. Cosmochim. Acta* **66**, 3955–3969.

Sessions A. L., Sylva S. P., Summons R. E. and Hayes J. M. (2004) Isotopic exchange of carbon-bound hydrogen over geologic timescales 1 1Associate editor: J. Horita. *Geochim. Cosmochim. Acta* **68**, 1545–1559.

Steinsbu B. O., Thorseth I. H., Nakagawa S., Inagaki F., Lever M. A., Engelen B., Ovreas L. and Pedersen R. B. (2010) Archaeoglobus sulfaticallidus sp. nov., a thermophilic and

facultatively lithoautotrophic sulfate-reducer isolated from black rust exposed to hot ridge flank crustal fluids. *Int. J. Syst. Evol. Microbiol.* **60**, 2745–2752.

Stouthamer A. H. and Bettenhaussen C. W. (1977) A continuous culture study of an ATPase-negative mutant of Escherichia coli. *Arch. Microbiol.* **113**, 185–189.

Thauer R. K. (2012) The Wolfe cycle comes full circle. *Proc. Natl. Acad. Sci.* **109**, 15084–15085.

Valentine D. L. (2007) Adaptations to energy stress dictate the ecology and evolution of the Archaea. *Nat. Rev. Microbiol.* **5**, 316–323.

Van Der Meer M. T. J., Benthien A., French K. L., Epping E., Zondervan I., Reichart G.-J., Bijma J., Sinninghe Damsté J. S. and Schouten S. (2015) Large effect of irradiance on hydrogen isotope fractionation of alkenones in Emiliania huxleyi. *Geochim. Cosmochim. Acta* **160**, 16–24.

Wakil S. J., Stoops J. K. and Joshi V. C. (1983) FATTY ACID SYNTHESIS AND ITS REGULATION.

Wijker R. S., Sessions A. L., Fuhrer T. and Phan M. (2019) ^{2}H/ ^{1}H variation in microbial lipids is controlled by NADPH metabolism. *Proc. Natl. Acad. Sci.* **116**, 12173–12182.

Wolfshorndl M., Danford R. and Sachs J. P. (2019) 2H/1H fractionation in microalgal lipids from the North Pacific Ocean: Growth rate and irradiance effects. *Geochim. Cosmochim. Acta* **246**, 317–338.

Wu W., Meador T. B., Könneke M., Elvert M., Wegener G. and Hinrichs K. (2020) Substrate-dependent incorporation of carbon and hydrogen for lipid biosynthesis by *Methanosarcina barkeri*. *Environ. Microbiol. Rep.* **12**, 555–567.

Zhang X., Gillespie A. L. and Sessions A. L. (2009) Large D/H variations in bacterial lipids reflect central metabolic pathways. *Proc. Natl. Acad. Sci.* **106**, 12580–12586.

Zhang Z. and Sachs J. P. (2007) Hydrogen isotope fractionation in freshwater algae: I. Variations among lipids and species. *Org. Geochem.* **38**, 582–608.